Regulation of Rab5 Activation Cycle during Macropinocytosis and Phagocytosis

by

William David Feliciano

A dissertation submitted in partial fulfillment
of the requirements for the degree of
Doctor of Philosophy
(Cellular and Molecular Biology)
in The University of Michigan
2011

Doctoral Committee:

Professor Joel A. Swanson, Chair
Professor Lois S. Weisman
Professor Robert S. Fuller
Associate Professor Kristen J. Verhey
Assistant Professor Erik E. Nielsen

To All My Family and Friends

Acknowledgments

A special thanks to Professor Joel A. Swanson for being a great teacher, advisor and motivator. Thanks for all his support and guidance and lots of thanks for his tolerance and understanding.

Thanks to all of the members of the Swanson Lab and the Center for Live Cell Imaging. Their level of expertise and their willingness to help and share that knowledge was critical for the completion of my thesis. Thanks to Dr. Adam Hoppe and Dr. Samuel W. Straight for teaching me all the microscopy methods used in this thesis and to Ladislaus Dombrowski for his help with the software used for processing the data. Also I want to thank Suresh Mohan for his help with the experiments for the chapter 4 project and Dr. Sei Yoshida for his data that forms part of Fig. 3.6.

Finally I want to thank God for bringing such amazing people to my life and my family, whose support was key for this achievement.

Table of Contents

List of Figures

Figure

List of Abbreviations

Abbreviations

PC – Image phase-contrast.

I_A – Image of acceptor excitation, acceptor emission.

I_D – Image of donor excitation, donor emission.

I_F – Image of donor excitation, acceptor emission.

I_R – Image of volume marker excitation, volume marker emission.

α, β – Calibrations from free acceptor and free donor respectively, which correct for spectral crossover into the I_F image.

γ - Calibration obtained from a linked construct of known FRET efficiency; the ratio of the extinction coefficients of the acceptor to the donor at the donor excitation.

ξ - Calibration obtained from a linked construct of known FRET efficiency; a proportionality constant relating the increase in sensitized acceptor emission to the decrease in donor fluorescence due to FRET.

SE – Sensitized emission, acceptor fluorescence due to resonance energy transfer from the donor.

A – Image of the total fluorescence of the acceptor.

D – Image of the total fluorescence of the donor.

EDA – Image of the total concentration of donor-acceptor in complex times the FRET efficiency.

E_A – Image of the fraction of acceptor in complex times the FRET efficiency.

E_D – Image of the fraction of the donor in complex times the FRET efficiency.

E_{AVG} – Image of the average of the fraction of acceptor in complex (E_A) plus the fraction of donor in complex (E_D).

R_{XX} – Image of the ratio of acceptor or donor to volume marker.

EO – Image, E_{AVG} image thresholded with binary masks made from D images. The masks were thresholded to identify only the CFP-Rab5a-positive organelles and a pseudocolor scale was applied to the masked E_{AVG} images, two pseudocolor scales applied (A) assigning different colors at 5% E_{AVG} steps (0 to 40% E_{AVG}) or (B) a threshold set to red for values below a given E_{AVG} and green above that E_{AVG}.

TO – Image, EDA images were averaged and the average noise subtracted from the original EDA images. These were then eroded and dilated in Metamorph to improve visualization of the active Rab5a-positive tubules. These were overlaid as green on the phase-contrast images.

E_{AVG}Max – Maximum level of E_{AVG} reached by the macropinosome.

Lm – Listeria monocytogenes

hly – Listeria monocytogenes gene that encodes the pore-forming cytolysin Listeriolysin O.

LLO – Pore-forming protein Listeriolysin O.

BMM – Bone marrow-derived macrophages.

RBD – Rab5-binding domain.

PI3P – Phosphatidylinositol 3-phosphate.

GEF – Guanine nucleotide exchange factor.

GAP – GTPase-activating protein.

GDI – GDP-dissociation inhibitor.

EGF – Epidermal growth factor.

M-CSF – Macrophage colony-stimulating factor.

YFP- Yellow fluorescent protein.

CFP – Cyan fluorescent protein.

RBC – Red blood cells.

FRET – Förster resonance energy transfer.

Abstract

Infection *by Listeria monocytogenes* involves escape from its phagocytic compartment prior to fusion with the lysosome. Previous studies show that small GTPase Rab5a plays a crucial role in *Lm* ability to escape from its compartment and that *Lm* is able to modulate Rab5a activity, promoting GDP exchange of Rab5a. Rab5a regulates the homo- and heterotypic fusion of membranous organelles during the early stages of endocytosis. The extent to which molecules that regulate Rab5a coordinate its cycling on membranes to affect the behavior of individual organelles has not been determined. This study used novel Förster Resonance Energy Transfer (FRET) microscopic methods to analyze the Rab5a cycle on macropinosomes and phagosomes, two large endocytic vesicles that form in ruffled regions of cell membranes. In Cos-7 cells and mouse macrophages stimulated with growth factors, Rab5a activation followed immediately after its recruitment to newly formed macropinosomes. Rab5a activity increased continuously and uniformly over macropinosome membranes then decreased continuously, with Rab5a deactivation preceding dissociation by 1-12 min. Maximal levels of Rab5a activity was independent of organelle size, but Rab5a cycles were longer on larger macropinosomes, consistent with an integrative activity governing Rab5a dynamics on individual organelles. The Rab5a cycle was destabilized by microtubule depolymerization and by bafilomycin A1. Overexpression of activating and inhibitory proteins indicated that active Rab5a stabilized macropinosomes. Thus, overall Rab5a activity on macropinosomes is coordinated by macropinosome structure and physiology. In macrophages Rab5a showed different levels of FRET on *Lm*-containing vacuoles. Macropinosomes that formed secondary to the phagocytic events showed higher FRET levels than during RBC and *Lm* phagocytosis. During uptake of *hly*- and heat-killed *Lm*, Rab5a localized to the vacuole with low FRET

levels, which points to a possible role of LLO. During vesicle fusion events Rab5a FRET was higher at the point of contact of the vacuoles and increased over the whole organelle after fusion implying two distinct regulatory events. Thus, as on macropinosomes Rab5a plays a role in phagocytosis but requires lower levels of activation. *Lm* affects Rab5a activation cycling although currently we are not able to elucidate if *Lm* vacuoles with low FRET levels have higher survival rates.

Chapter I

Introduction

Endocytosis

Endocytosis is a process by which cells take up liquids, nutrients or particles from the extracellular medium. This process is commonly divided into three distinct categories: receptor-mediated endocytosis, pinocytosis and phagocytosis. During endocytosis, the cell extends an actin-rich membrane protrusion or ruffle around its particulate cargo and closes by fusing at the distal edges (1). Once internalized, the new compartment undergoes a maturation process which leads to acidification of the compartment by vacuolar-type H^+-ATPase, recruitment of compartment-specific membrane proteins and production of compartment-specific phosphoinositides. The internalized compartment fuses with early endosomes, which have a tubulo-vesicular shape, a pH of about 6.5 and specific membrane GTPases such as Rab5 and Rab4. The phosphoinositide composition is also changed by Class III phosphatidylinositol-3 kinase (PI3K), which produces phosphatidylinositol 3-phosphate (PI3P) from phosphatidylinositol. At this stage some receptors are recycled back to the membrane via Rab4-positive vesicles. As the early endosome matures into a late endosome, its internal pH decreases to 5.5 and it acquires Rab7 and Rab9. Its membrane phosphoinositide composition also changes from PI3P to $PI(3,5)P_2$. The final stage in the process is fusion of the late endosome with the lysosome. The pH is 4.5 – 5.0 and the cargo is degraded by hydrolases into simple compounds which are then used as nutrients or for antigen presentation.

Macropinocytosis

Macropinocytosis is the mechanism by which cells internalize large volumes of extracellular medium into 0.2 to 10 μm diameter vesicles. Some cell types form macropinosomes spontaneously, while others require stimulation by growth factors. For example, macrophages undergo macropinocytosis when stimulated with macrophage colony-stimulating factor (M-CSF) or with phorbol esters (2). Macropinosome closure involves two events. First, a cell surface ruffle curves into a circular ruffle, forming a cup-shaped protrusion from the cell (ruffle closure). Second, the macropinocytic cup closes at its distal margin, forming an intracellular vacuole, the macropinosome (cup closure). Previous studies have identified roles for Class 1A PI3K and different small GTPases in macropinosome formation (3). Rac-1, for example, regulates remodeling of the actin cytoskeleton during ruffling in response to epidermal growth factor (EGF) in epithelial cells (4). M-CSF-induced macropinocytosis depends on Rac1 and the Rac1-binding protein WAVE2 (4). Rac1 and Cdc42 activate p21-activated kinase-1 (Pak1), which may facilitate fission of the membrane by phosphorylation of CtBP1/Bars during macropinocytosis (5). Cdc42 and Arf6 also play important roles during macropinocytosis in macrophages, affecting actin cytoskeleton rearrangement during stimulation with M-CSF (6). Another GTPase involved in signal transduction and macropinocytosis is Ras, which interacts with Rin1, a Rab5 GDP/GTP exchange factor (GEF) (7). Overexpression of Ras causes an increase in macropinocytosis (8). As macropinosomes mature inside cells, they acquire endosomal markers such as Rab5, Rab7 and Lamp1 and either fuse with lysosomal compartments or recycle to the cell surface.

Phagocytosis

Phagocytosis is an important process by which cells internalize particles larger than 1 μm in diameter. The cell which contacts a particle recognizes it in one of two ways. In non-opsonic phagocytosis, receptors bind to specific

common molecular motifs on the surface of particle, such as carbohydrates (9). These motifs or pathogen-associated molecular patterns are specific non-variable sequence targets which the host species has encountered in its evolutionary past (9). Pathogens have evolved ways to change these patterns to avoid detection by the host. Conversely, host cells use a combination of receptors during phagocytosis to improve their ability to recognize pathogens. In opsonic receptor-mediated phagocytosis, phagocytic receptors bind to antibodies or complement fragments which decorate (opsonize) the surface of the particle. Pathogens may encounter five different classes of opsonizing immunoglobulin antibodies: IgM, which is expressed on the surface of B cells or as a secreted molecule; IgA, which is found in mucosal areas of the body; IgD, which is involved in binding by naïve B cells; IgE, which is also commonly found in mucosal areas and which plays a role in allergen recognition and histamine release; and IgG, which is the major immunoglobulin involved in pathogen-directed humoral immunity (10). Antibodies differ in their heavy chains, which are referred to as μ, δ, γ, α and β. These differences in their heavy chains are recognized by specific receptors on the surface of immune cells. Of the phagocytic receptors which recognize immunoglobulins, the Fcγ receptor (FcR) is the most studied (11). Of the three classes of FcR - FcγRI, FcγRII and FcγRIII - FcγRI has the highest binding affinity to IgG. Phagocytosis of IgG-opsonized particles via FcR occurs through interactions of cytosolic proteins with the immunoreceptor tyrosine-based activation motifs (ITAMs) in the cytoplasmic domain of the Fc receptor. Phagocytosis can also be inhibited by receptors containing immunoreceptor tyrosine-based inhibitory motifs (ITIMs) in their cytoplasmic domains (12).

Listeria monocytogenes

The human pathogen *Listeria monocytogenes* (*Lm*) is a facultative intracellular gram-positive bacterium. In epithelial cells, internalin molecules on *Lm* bind to host cell adhesion factors, such as E-cadherin, which interact with α-

and β-catenin to effect actin cytoskeleton rearrangement (13). E-cadherin activates the Rho-family GTPases Rho, Rac1 and Cdc42, stabilizing Wiskott Aldrich syndrome protein (WASP), which binds the Arp2/3 complex serving as an actin nucleation point (14). These first steps lead to membrane extension around *Lm* and engulfment. Within 30 minutes after uptake, the vesicle membrane lyses, allowing *Lm* to escape into the host cell cytoplasm (Fig. 1.1). This escape event involves three virulence factors: the hemolysin listeriolysin O (LLO), which forms pores on the membrane and phospholipases A and B, which break down membrane phospholipids and disrupt the vacuolar membrane. *Lm* replicates only in the cytoplasm. Once it has replicated, it expresses its virulence factor ActA, which binds the Arp2/3 complex of the cell and induces actin nucleation. Actin polymerization occurs on a specific area of the bacterium, propelling it through cytoplasm and into the host cell membrane. Actin-based *Lm* motility forms a protrusion at the cell surface which leads to internalization by a neighboring cell. In this second cell, the bacterium is enclosed in a double-membrane vacuole. This mode of direct cell-to-cell spread is known as paracytophagy (15).

Host defense is composed of protective systems that guard against infection by pathogenic bacteria and viruses; these systems include physical anatomical barriers and the immune system. The immune responses can be divided into two types: innate and adaptive. In an innate immune response, which is generally the first response, cells respond in a generic way to pathogens. This type of response is often unable to completely clear the infection. The second type of host defense is the adaptive or specific immune response. It comprises highly specialized cells and processes that eliminate pathogens or prevent their growth. The latter response occurs after the innate immune response and confers a memory of specific pathogens by recognizing specific domains of pathogenic proteins and expanding populations of lymphocytes with specific receptors for pathogen-associated molecules. This helps the immune system to mount stronger attacks in subsequent infections by the pathogen.

Both macropinocytosis and phagocytosis are involved in the host's immune responses. During infections, phagocytosis is carried out by neutrophils, dendritic cells and macrophages. In response to signals released during an inflammatory response, these cells localize to the site of damage or infection, ingest the pathogen by phagocytosis and kill it using molecules such as reactive oxygen intermediates. Pathogen-derived protein degradation products are presented at phagocyte cell surfaces to initiate or stimulate adaptive immune responses. These antigens are presented to T cells which then stimulate B cells to produce antibodies specific for the pathogen. The antibodies may contribute later to receptor-mediated phagocytosis. Macropinocytosis is used by dendritic cells to sample the extracellular environment for foreign proteins. These proteins are internalized and cleaved to generate peptides that are recycled to the cell surface as MHC class II-peptide complexes or delivered to the cytosol for subsequent presentation on MHC class I molecules.

Rab5

Rab5 is a member of the Rab family of small GTPases, which is a subgroup of the Ras GTPase superfamily. The GTPases of this superfamily cycle between inactive, GDP-bound forms and active, GTP-bound forms (Fig. 1.2). They are activated by GDP/GTP exchange factors (GEFs) and inactivated by GTPase-activating proteins (GAPs). In their GTP-bound form, they interact with various effector proteins. The differential affinity of the GTP-bound and GDP-bound GTPases for their effector proteins permitted the development of biochemical and FRET-based methods for measuring and localizing GTPase activation in cells.

Rabs regulate docking and fusion in the endocytic and secretory pathway. Three isoforms of Rab5: a, b and c, overlap in their intracellular distributions. Rab5 has been found to be the rate-limiting molecule for endocytosis (16) and is involved in the translocation and activation of Rac2, leading to the oxidative burst (17). In its GTP-bound form, Rab5a facilitates both the fusion of endocytic

vesicles with early endosomes and the homotypic fusion of early endosomes (Fig. 1.3). Previous work in our laboratory, using fluorescent chimeras of Rab5a and ratiometric fluorescence microscopy, showed that the maturation pathway in macrophages presents proteins on phagosomes, including actin, Rab5a, Rab7 and LAMP1 (18). Other groups showed that the inhibition of Rab5a by pathogens could alter the progression of phagosomes to lysosomes and also that mutations of the Rab5 gene or its activating or inhibitory proteins result in human diseases such as Alzheimer's and Huntington's, indicating its importance in infectious and neurological diseases (19-24).

Rabaptin-5 is a Rab5 effector that has been shown to interact with active Rab5 via Rabaptin-5's C-terminal domain (aa 551-862) (25, 26). Previous work has also shown that it is recruited to early endosomes. It is involved in stabilization of active Rab5 and is required for fusion between endosomes. Early Endosome Antigen-1 (EEA1) is another Rab5 effector which interacts with active Rab5 via both its N- and C-terminals and is required for endosome fusion (27). It contains a FYVE domain on its C-terminal that interacts specifically with PI3P.

Some pathogens have evolved mechanisms to interfere with crucial steps of phagocytosis. Some delay phagosome fusion with the lysosome, others escape from the phagosome into the cytoplasm (17). Some pathogens exploit Rab5 function to enhance intracellular survival. *Salmonella enterica* var. *Typhimurium*, for example, utilizes one of its virulence factors, SopE, which recruits Rab5 and, as a Rab5 exchange factor, keeps Rab5 in its active form, thereby promoting fusion with endosomes and delaying fusion with the lysosome (17). Phagosomes containing *Legionella pneumophila* lack Rab5, which may explain their limited interaction with other endocytic compartments (20). On the other hand, phagosomes containing *Mycobacterium tuberculosis* have persistently active Rab5, which may explain the delay in fusion of the phagosome with the lysosome (20).

Rab5 may also contribute to *Lm* survival inside macrophages. Active Rab5 expression correlates with *Lm* phagosome maturation (18). Modulation of the GDP to GTP exchange step of Rab5a is a possible mechanism used by the

bacterium to avoid degradation (28). Rab5 localization to the *Lm*-containing vacuole could be cell type-specific. Henry, et al., (29) showed that in the RAW 264.7 macrophage cell line, Rab5 did not localize to the *Lm*-containing vacuole; whereas Alvarez-Dominguez, et al., (30) saw localization of Rab5 to the *Lm*-containing vacuole in J774E and CHO cells.

Ratiometric Microscopy

The main goal of this work was to build a FRET system that would allow us to study the Mass Rab5 Cycle *in vivo* and the effect that different activating and inhibitory proteins of Rab5 have on the net organelle cycle and on macropinosome dynamics (Fig. 1.4). With this novel system, we could observe the aggregate behavior of Rab5 on the entire organelle and measure the four major steps of Rab5: 1) association, 2) activation, 3) deactivation and 4) dissociation from the membrane (Fig 1.2) (31).

Cos-7 cells were co-transfected with plasmids encoding YFP-RBD, CFP-Rab5a and pIRES2-mCherry. mCherry served as a cytosolic volume marker which corrected for optical pathlength due to cell shape (Fig. 1.5). A total of five images were acquired: Phase-contrast, I_A, which contains the FRET-independent fluorescence from the acceptor, I_D, which contains the fluorescence from the donor, I_F, which contains a mixture of donor, acceptor and FRET signals and I_R, which contains the fluorescence from mCherry. To acquire these images we used a Nikon TE300 widefield inverted fluorescence microscope and the program MetaMorph version 7.7r1 (Molecular Devices, Sunnyvale, CA).

Ratiometric measurements were calculated for each cell using MATLAB R2009a (The Mathworks, Natick, MA), the DIPImage toolbox for MATLAB (http://www.diplib.org, Quantitative Imaging Group, Delft University of Technology, Netherlands) and FRET Calculator (available from the Center for Live Cell Imaging at the University of Michigan) and images were corrected for exposure times and shade and bias corrections during processing (Abbreviation

definitions on page 10). Ratiometric images of CFP-chimeras were calculated from two images, the CFP-Rab5 image I_D, and mCherry image I_R (32). The ratio of CFP-chimera to mCherry was calculated by dividing each pixel of the CFP-Rab5 image by the corresponding pixel in the mCherry image, this reported the localization of Rab5 normalized to cell volume in a monochromatic image. A pseudocolor scale was added to the ratio image where low ratio values are represented by cool color and high ratio values by warm colors (Fig 1.6). The results obtained with ratiometric microscopy allow us to observe Rab5 dynamics but not differentiate between active and inactive Rab5. To differentiate we used FRET.

FRET stoichiometry

Förster resonance energy transfer occurs when two fluorescent protein chimeras, one containing a donor fluorophore and the other containing an acceptor fluorophore, come into contact with each other (33). The average distance between fluorophores necessary for resonance energy transfer is 6-10 nm. When a donor fluorophore is excited at its excitation optimum it emits light at a lower wavelength that results in a donor image. The same principle occurs when an acceptor flourophore is excited. When these two fluorophores come close to each other, however, one can excite the donor and obtain an image of FRET at the acceptor's wavelength. This is because the donor's emission maximum is at the same wavelength for acceptor excitation (by design). Some of the resonance energy emitted by the donor is absorbed by the acceptor fluorophore, exciting it and causing the emission of acceptor fluorescence at its emission wavelength (Fig 1.7). The image obtained by exciting at the donor's wavelength and reading at the acceptor's emission wavelength is the FRET image, which contains a mixture of fluorescence from directly excited donor, directly excited acceptor and acceptor excited by FRET.

FRET stoichiometry was used to measure the proportions of donor, acceptor and donor-acceptor complex in each pixel. FRET calibration

parameters were determined using Cos-7 cells expressing YFP only (α), CFP only (β) or a linked YFP-CFP molecule of known FRET efficiency (γ and ξ). These calibrations take into account the crossover of the emission wavelengths of each fluorophore and energy transfer effect on the FRET pairs, allowing us mathematically to subtract these signals and to obtain quantifiable FRET measurements. The FRET Calculator was used to obtain the total concentrations of acceptor (A) and donor ($D = I_D + EDA*\xi$), the FRET efficiency times the concentration of donor-acceptor complex ($EDA = I_F - \alpha*I_A - \beta*I_D$), the fraction of the acceptor in complex times the FRET efficiency (E_A), the fraction of the donor in complex times the FRET efficiency (E_D), the average FRET efficiency ($E_{AVG} = (E_A+E_D)/2$), the ratio of acceptors to cytoplasmic marker (R_{YR}), the ratio of donors to cytoplasmic marker (R_{CR}) and molar ratio of acceptors to donors (R_M).

When studying and comparing the total Rab5 and the active Rab5 signals we used the D and EDA images, both images are qualitative intensity images. For quantitative measurements of Rab5 FRET, we used the E_{AVG} image instead of the E_A or E_D images because E_{AVG} is independent of the differences in concentration levels due to transient transfections, a more accurate FRET value (33-35). The EO image was created by thresholding the E_{AVG} image with binary masks made from D images. The masks were thresholded to identify only the CFP-Rab5a-positive organelles. Two new scales were then applied to the masked E_{AVG} images: a pseudocolor scale assigning different colors at 5% E_{AVG} steps (0 to 40% E_{AVG}), or another thresholded with two different binaries from D images. For example, in some images the threshold was set to red for E_{AVG} values from 0–8% and green from 8–40%. The new scaled images were then overlayed onto the phase-contrast images (Fig. 1.8). The maximum FRET level is 40%; this was calculated using a linked construct of the donor and acceptor at a known FRET efficiency. E_{AVG}Max is the highest level of Rab5 FRET reached by the organelle and was used to compare the different uptake events and cycle modulation. The TO images were created by averaging the EDA images and subtracting the average noise from the original EDA images, the new EDA images were eroded and dilated in Metamorph to improve visualization of the

active Rab5a-positive tubules. The images were then overlaid as green on phase-contrast images.

pIRES System

To study how different Rab5 GEFs and GAPs affect its Mass cycle and to facilitate ratiometric and FRET studies in the same cell, we constructed a library of pIRES2-mCherry vectors that express different proteins known to be involved in endocytosis (Fig 1.9). The pIRES2 vector contains an internal ribosomal entry site (IRES) between its multiple cloning site and the fluorophore site which allows the translation of both in a single bicistronic mRNA (Fig 1.10). The mCherry allowed for detection of cells transfected with non-fluorescent proteins and Rab5-modifying proteins (GAPs and GEFs).

Thesis Overview

The previous background leads to the focus of my thesis and the main questions I try to answer. Rab5 is a crucial protein for vacuole trafficking that has been targeted through evolution by pathogenic microorganisms. How is the chemistry of Rab5 organized on individual organelles? How does *Lm* modify that chemistry for pathogenesis? To address these questions, I have organized my thesis into two parts: the characterization of the Rab5 activity cycle on individual vacuoles and the analysis of Rab5 activity on macropinosomes, phagosomes and *Lm*-containing vacuoles. To do this, I developed new tools and methods to study the Rab5 cycle *in vivo*. This involved characterization of two Rab5 FRET partners: the amino terminal Rab5-binding domain of EEA1 and the Rab5-binding domain from the Rab5 effector Rabaptin-5 (25, 27). A second tool combined FRET and ratiometric microscopy, allowing me to obtain large amounts of information about GTPase cycling on individual organelles. A third tool was the pIRES2-mCherry library containing Rab5 GAPs and GEFs or functional mutants of Cdc42, Rac1, Rac2, Arf1 and Arf6. These allowed me to

study the effects of interfering with these proteins on Rab5 dynamics. Lastly, I developed methods to observe the uptake of *Lm*, which allowed me to study through live cell imaging the organization of the Rab5 cycle and the effect of *Lm* on Rab5 activity on the *Lm* vacuole. I used these tools to analyze the Rab5 cycle in macropinocytosis, phagocytosis and infection of macrophages by *Lm*. Through study of the role of Rab5 on the *Lm*-containing vacuole and the complexity of its effects on the endocytic pathway, it is hoped that these tools will lead to better understanding of pathogen biology and to the eventual identification of pharmaceutical targets of infection.

Figure 1.1. *Listeria monocytogenes* Life Cycle. Murine bone marrow-derived macrophage infected with *Lm* were fixed and immunostained for actin using Texas red-phalloidin (red) and for DNA using DAPI (blue). Escaped *Listeria* show actin-polymer surrounding the bacteria; motile bacteria show actin-rich rocket tails (Left). Diagram depicting the life cycle of *Listeria* infection, indicating receptor-binding virulence factors that induce uptake of *Lm* by epithelial cells and role of pore-forming protein, listeriolysin O (LLO), during permeabilization of the vacuolar membrane and subsequent escape by the bacteria into the cytoplasm (36).

Figure 1.1

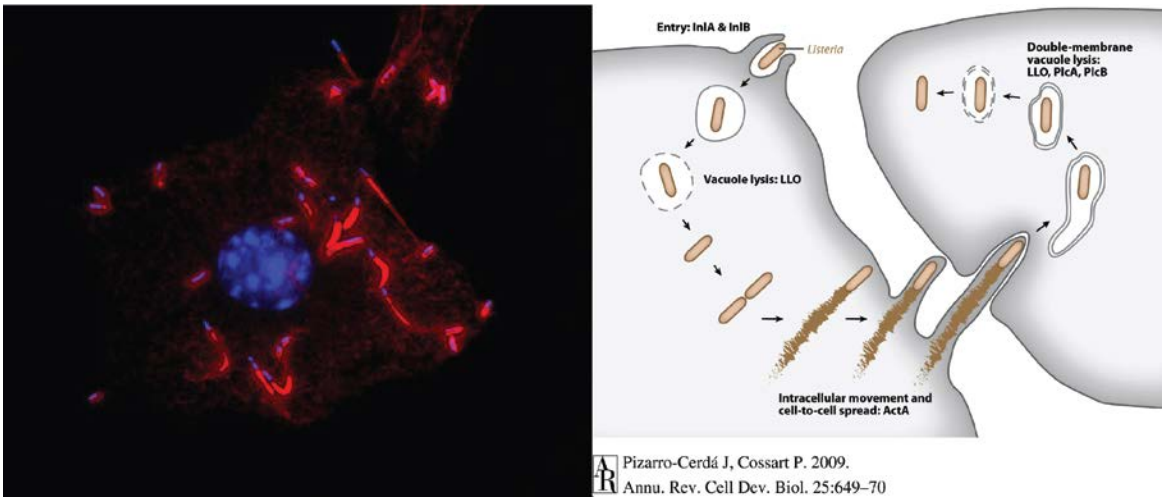

Pizarro-Cerdá J, Cossart P. 2009.
Annu. Rev. Cell Dev. Biol. 25:649–70

Figure 1.2. Rab5 Activation Cycle Diagram. Schematic of GTPase activation and deactivation. Active GTPase, ie., in its GTP-bound form, is able to recruit the necessary effectors. The GTPase is the deactivated by a GAP, through hydrolysis of GTP to GDP, and reactivated by a GEF (37).

Figure 1.2

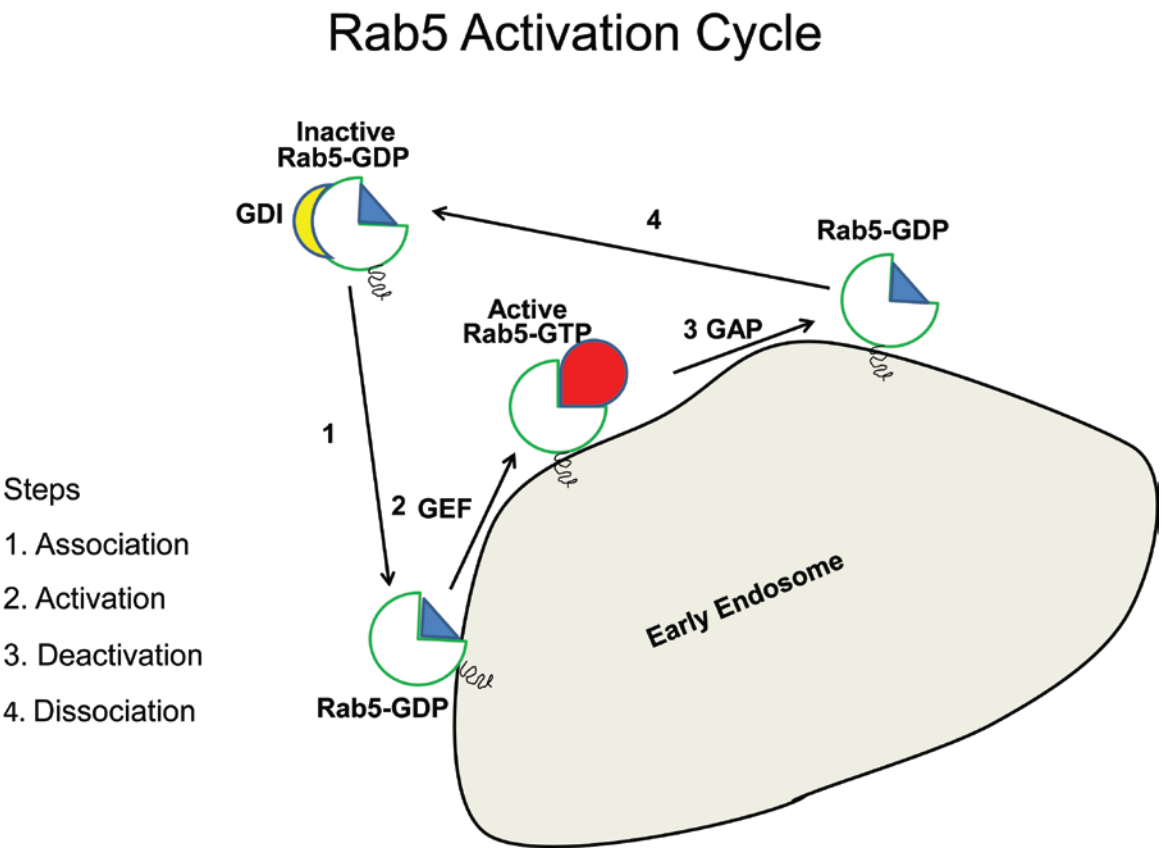
Rab5 Activation Cycle
Inactive
Rab5-GDP
GDI
4
Rab5-GDP
Active
Rab5-GTP
3 GAP
1
2 GEF
Steps
1. Association
2. Activation
3. Deactivation
4. Dissociation
Early Endosome
Rab5-GDP

Figure 1.3. The Rab5 Membrane Activity Cycle. Diagram describes Rab's role during vesicle budding from a donor compartment and fusion of the new vesicle with the acceptor compartment (38).

Figure 1.3

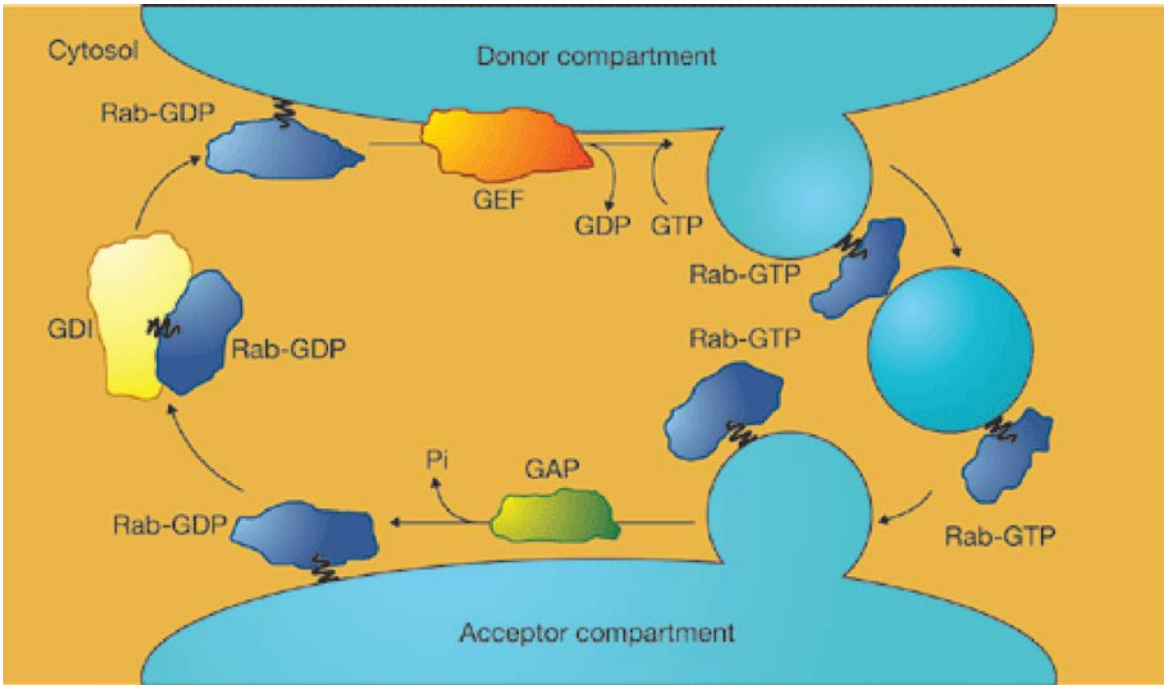
Cytosol
Donor compartment
Rab-GDP
GEF
GDP
GTP
Rab-GTP
GDI
Rab-GDP
Rab-GTP
Pi
GAP
Rab-GDP
Rab-GTP
Acceptor compartment

Figure 1.4. The net Rab5 cycle. The Rab5 FRET system measures the mass or aggregate behavior Rab5 on the membrane of macropinosomes which is composed of multiple Rab5 molecules undergoing activation and deactivation (Bottom). This system is not able currently to visualize single Rab5 molecule cycling (Top).

Figure 1.4

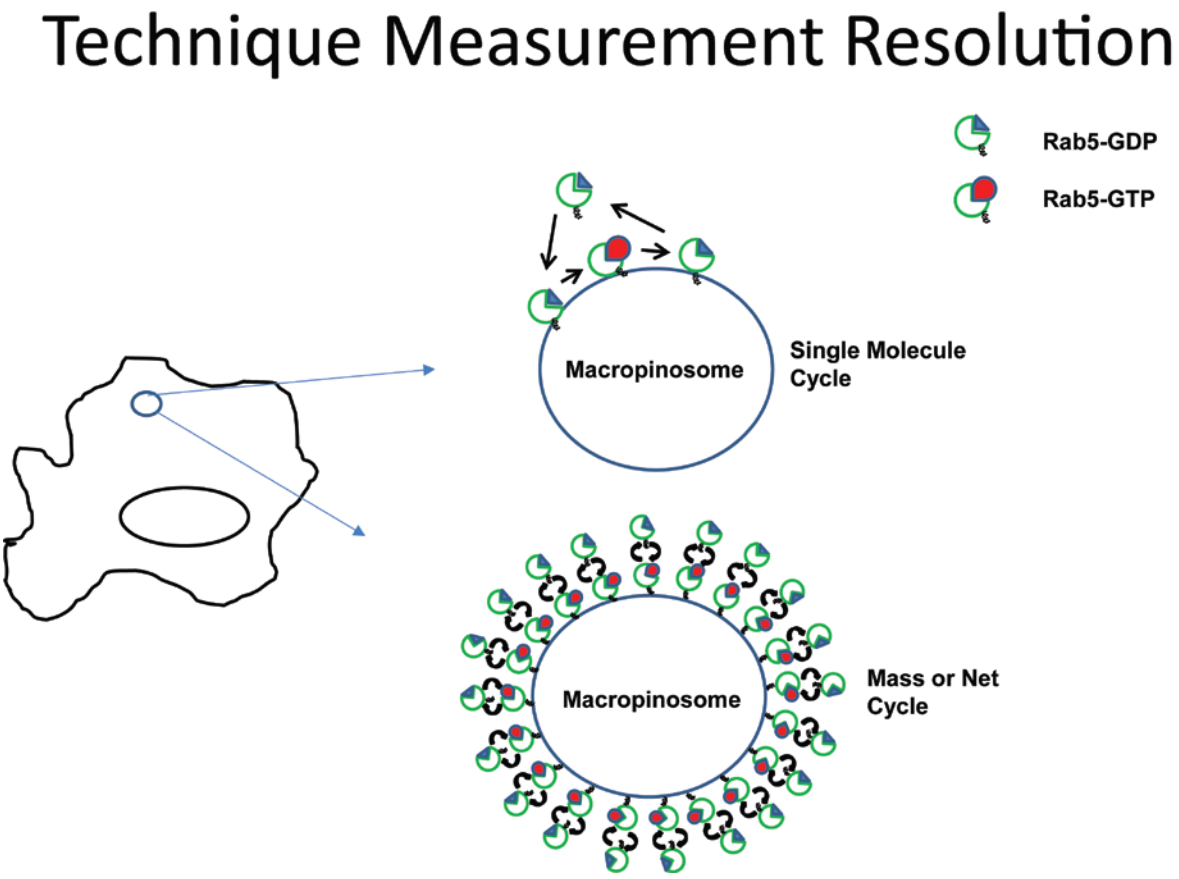
Technique Measurement Resolution
Rab5-GDP
Rab5-GTP
Macropinosome
Single Molecule Cycle
Macropinosome
Mass or Net Cycle

Figure 1.5. Three-color Transfection Diagram. Cells transfected with three different color constructs: 1) YFP-RBD 2) CFP-Rab5 and 3) mCherry-C1, pIRES2-mCherry or pIRES2-mCherry expressing a non-fluorescent protein. mCherry served as volume marker and was used to calculate the ratio of CFP-Rab5.

Figure 1.5

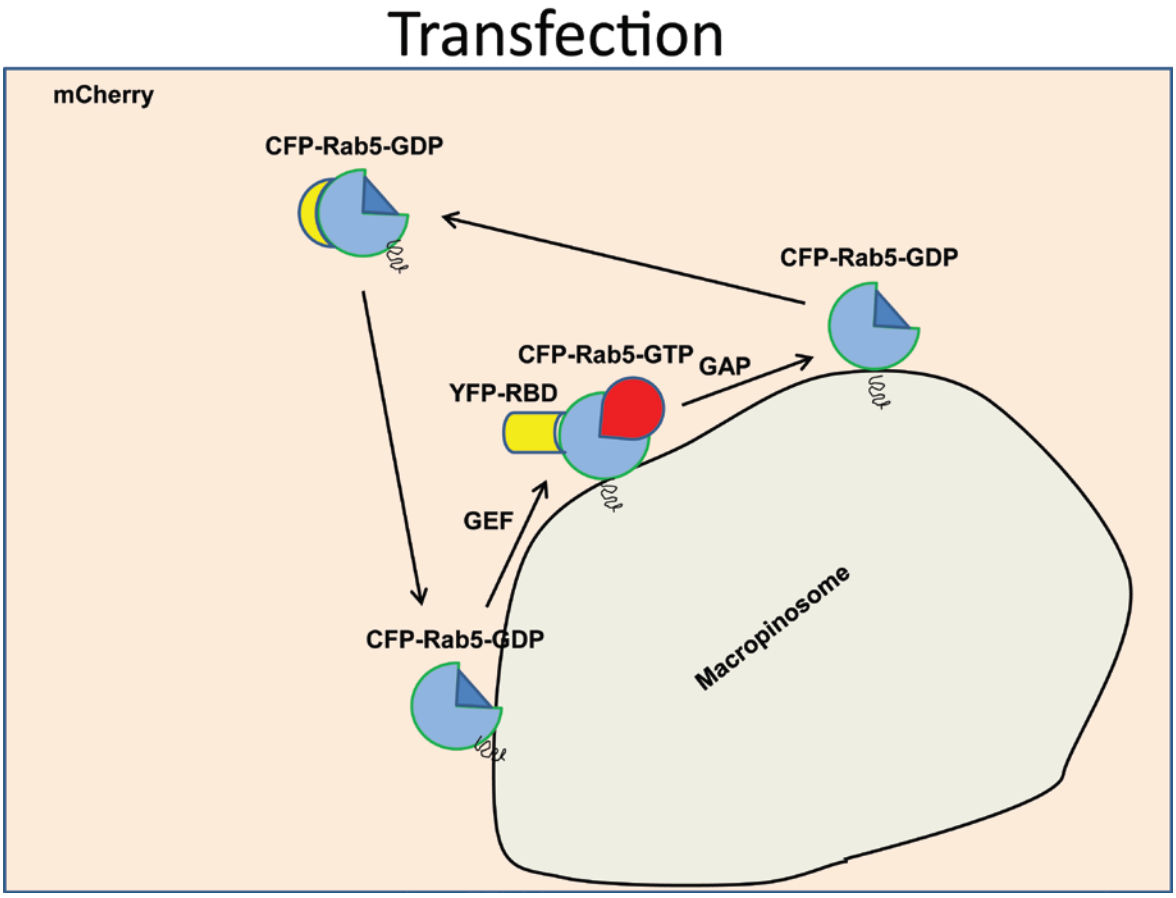
Transfection
mCherry
CFP-Rab5-GDP
CFP-Rab5-GDP
CFP-Rab5-GTP
GAP
YFP-RBD
GEF
CFP-Rab5-GDP
Macropinosome

Figure 1.6. Ratiometric Microscopy Processing. Ratio of CFP-chimera to mCherry was calculated by dividing each pixel of the CFP-Rab5 image by the corresponding pixel in the mCherry image. The result was a monochromatic ratio image to which a pseudocolor scale was added (low ratio values are represented by cool colors and high ratio values by warm colors).

Figure 1.6

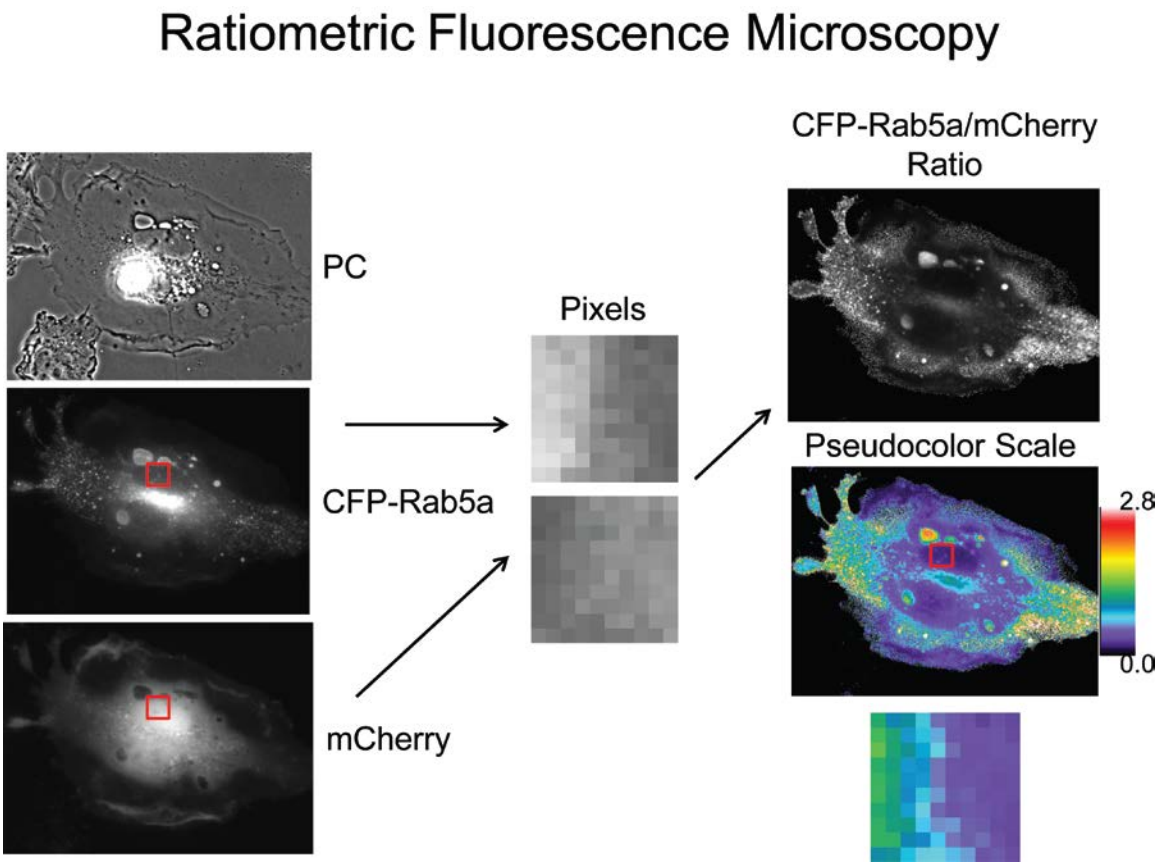
Ratiometric Fluorescence Microscopy
CFP-Rab5a/mCherry
Ratio
PC
Pixels
CFP-Rab5a
Pseudocolor Scale
2.8
0.0
mCherry

Figure 1.7. Förster Resonance Energy Transfer. FRET diagram shows two chimeras, one contains a donor fluorophore (CFP-Rab5) and another contains an acceptor fluorophore (YFP-RBD). When the proteins interact the fluorophores come close to each other (approximately 6 nm), the resonance energy of the excited donor fluorophore is transfered to the acceptor, exciting the acceptor and causing it to fluoresce.

Figure 1.7

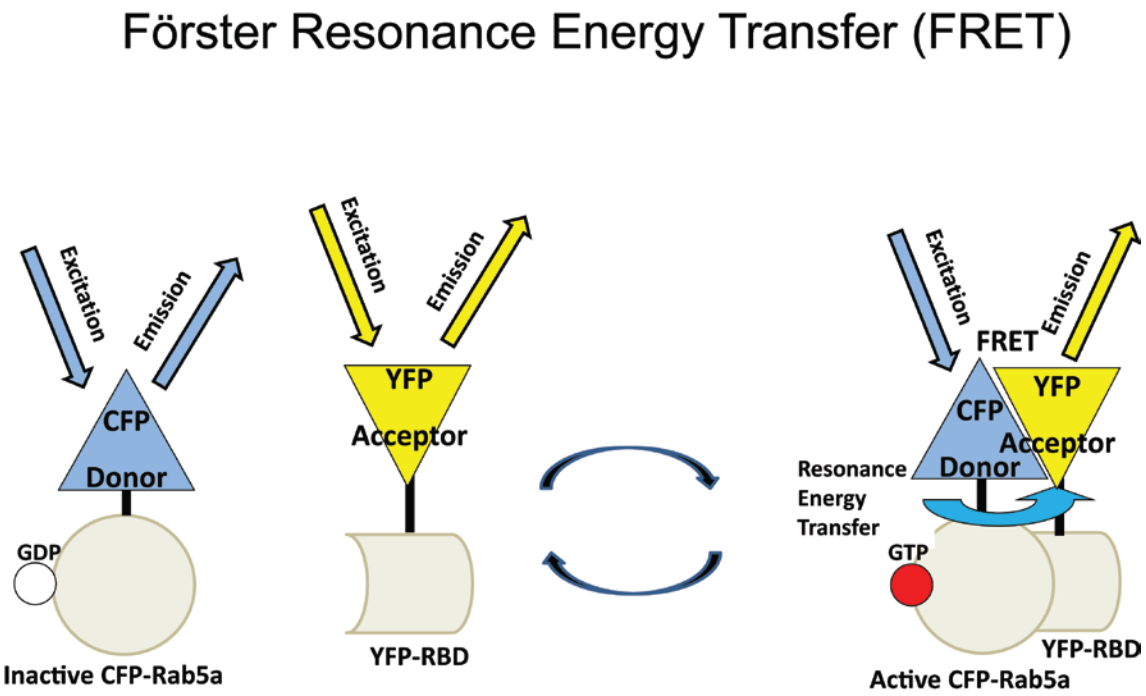
Förster Resonance Energy Transfer (FRET)
Excitation
Emission
CFP
Donor
GDP
Inactive CFP-Rab5a
Excitation
Emission
YFP
Acceptor
YFP-RBD
Excitation
Emission
FRET
YFP
CFP
Acceptor
Resonance
Energy
Transfer
Donor
GTP
YFP-RBD
Active CFP-Rab5a

Figure 1.8. FRET Stoichiometry Image Processing. The donor (I_D), acceptor (I_A) and FRET (I_F) images were processed using The FRET Calculator. The resulting images were D (total fluorescence of the donor), EDA (total concentration of donor-acceptor in complex times the FRET efficiency) and E_{AVG} (the average of the fraction of acceptor in complex (E_A) plus the fraction of donor in complex (E_D)). The D image was used to create a mask that only included the Rab5-positive organelles. Two new scales were applied to the E_{AVG} image, followed by application of the mask. The two new masked E_{AVG} images were then overlaid onto the phase-contrast image creating a new E_{AVG}-overlay image (EO).

Figure1.8

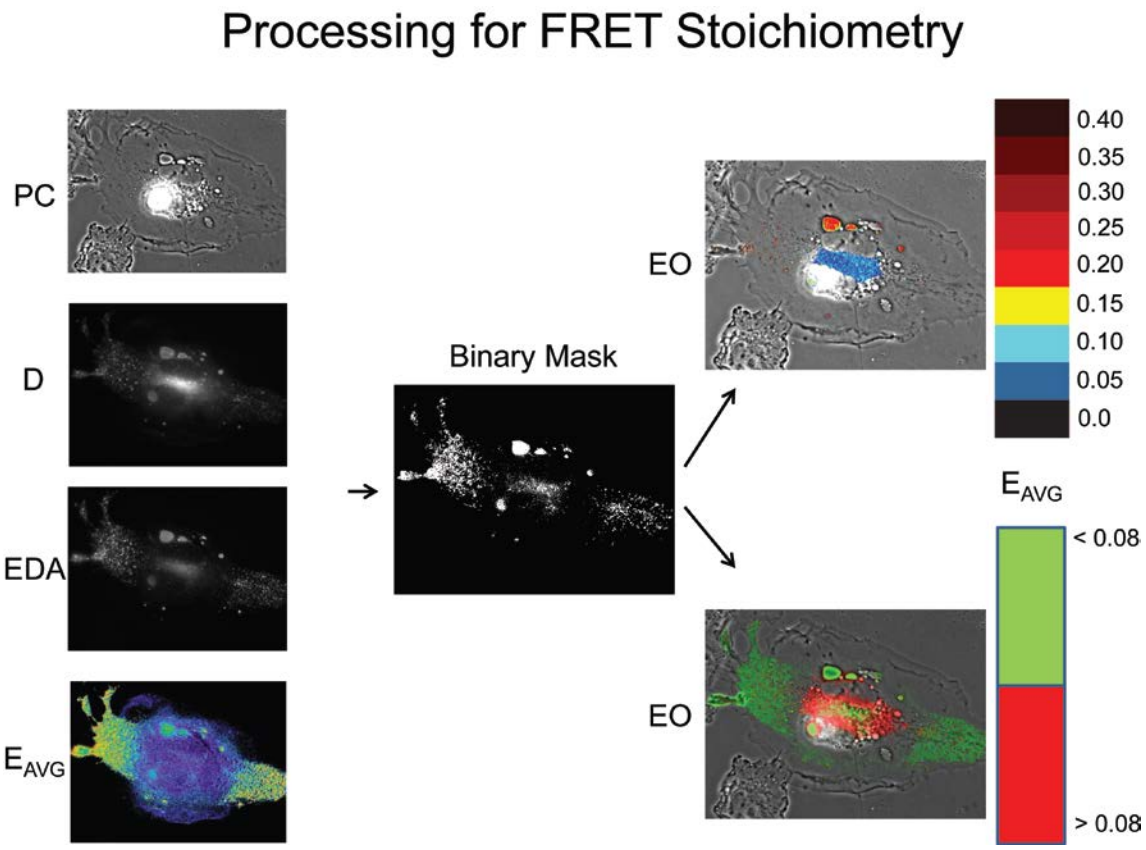
Processing for FRET Stoichiometry
PC
D
EDA
E_AVG
Binary Mask
EO
EO
0.40
0.35
0.30
0.25
0.20
0.15
0.10
0.05
0.0
E_AVG
< 0.08
> 0.08

Figure 1.9. pIRES2 System. A library was constructed composed of pIRES2-mCherry vector expressing wild-type, constitutively active and dominant negative versions of Arf6, Cdc42, Rac1 and Rac2, Rab5 GEFs Rin1 and Rabex-5 or Rab5 GAP RabGAP-5. The internal ribosome entry site allows the formation of a bicistronic mRNA which expresses two separate proteins, in this case mCherry and a non-fluorescent version of the previously mentioned proteins. This system allows us to use mCherry as a volume marker and as a transfection marker without affecting our ability to do ratiometric and FRET microscopy on single cells and the non-fluorescent protein to modulate or affect the Rab5 cycle.

Figure 1.9

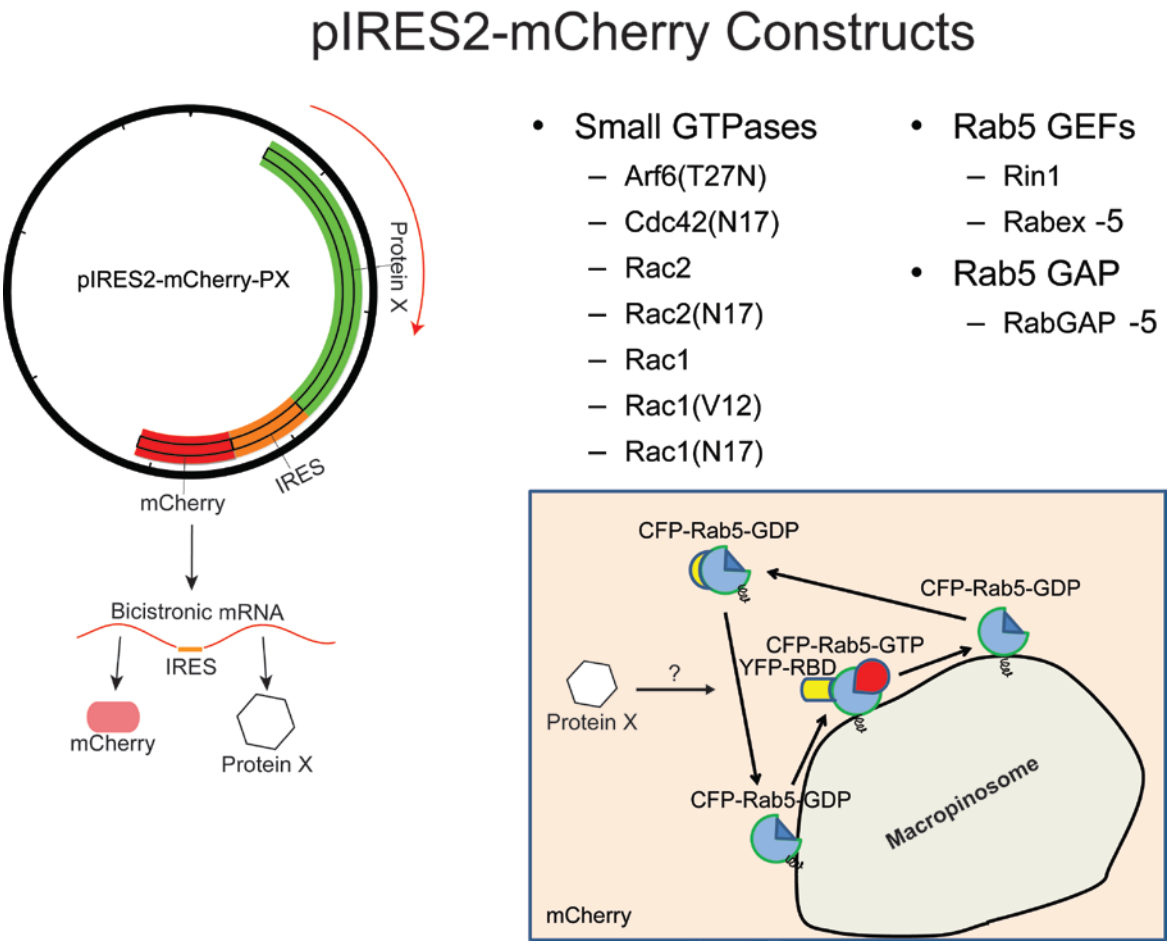
pIRES2-mCherry Constructs
pIRES2-mCherry-PX
Protein X
IRES
mCherry
Bicistronic mRNA
IRES
mCherry
Protein X
Small GTPases
Arf6(T27N)
Cdc42(N17)
Rac2
Rac2(N17)
Rac1
Rac1(V12)
Rac1(N17)
Rab5 GEFs
Rin1
Rabex -5
Rab5 GAP
RabGAP -5
CFP-Rab5-GDP
CFP-Rab5-GDP
CFP-Rab5-GTP
YFP-RBD
?
Protein X
CFP-Rab5-GDP
Macropinosome
mCherry

Bibliography

1. Swanson JA. Shaping cups into phagosomes and macropinosomes. Nat Rev Mol Cell Biol 2008;9(8):639-649.

2. Swanson JA, Yirinec BD, Silverstein SC. Phorbol esters and horseradish peroxidase stimulate pinocytosis and redirect the flow of pinocytosed fluid in macrophages. J Cell Biol 1985;100(3):851-859.

3. Falcone S, Cocucci E, Podini P, Kirchhausen T, Clementi E, Meldolesi J. Macropinocytosis: regulated coordination of endocytic and exocytic membrane traffic events. J Cell Sci 2006;119(Pt 22):4758-4769.

4. Kurokawa K, Itoh RE, Yoshizaki H, Nakamura YO, Matsuda M. Coactivation of Rac1 and Cdc42 at lamellipodia and membrane ruffles induced by epidermal growth factor. Mol Biol Cell 2004;15(3):1003-1010.

5. Liberali P, Kakkonen E, Turacchio G, Valente C, Spaar A, Perinetti G, Bockmann RA, Corda D, Colanzi A, Marjomaki V, Luini A. The closure of Pak1-dependent macropinosomes requires the phosphorylation of CtBP1/BARS. Embo J 2008;27(7):970-981.

6. Klein S, Franco M, Chardin P, Luton F. Role of the Arf6 GDP/GTP cycle and Arf6 GTPase-activating proteins in actin remodeling and intracellular transport. J Biol Chem 2006;281(18):12352-12361.

7. Galvis A, Balmaceda V, Giambini H, Conde A, Villasana Z, Fornes MW, Barbieri MA. Inhibition of early endosome fusion by Rab5-binding defective Ras interference 1 mutants. Arch Biochem Biophys 2009;482(1-2):83-95.

8. Porat-Shliom N, Kloog Y, Donaldson JG. A unique platform for H-Ras signaling involving clathrin-independent endocytosis. Mol Biol Cell 2008;19(3):765-775.

9. Kende M. Role of macrophages in the expression of immune responses. J Am Vet Med Assoc 1982;181(10):1037-1042.

10. Heggers JP. Natural host defense mechanisms. Clin Plast Surg 1979;6(4):505-513.

11. Gessner JE, Heiken H, Tamm A, Schmidt RE. The IgG Fc receptor family. Ann Hematol 1998;76(6):231-248.

12. Daeron M. Intracytoplasmic sequences involved in the biological properties of low-affinity receptors for IgG expressed by murine macrophages. Braz J Med Biol Res 1995;28(3):263-274.
13. Lecuit M, Hurme R, Pizarro-Cerda J, Ohayon H, Geiger B, Cossart P. A role for alpha-and beta-catenins in bacterial uptake. Proc Natl Acad Sci U S A 2000;97(18):10008-10013.
14. Ireton K, Cossart P. Host-pathogen interactions during entry and actin-based movement of Listeria monocytogenes. Annu Rev Genet 1997;31:113-138.
15. Robbins JR, Barth AI, Marquis H, de Hostos EL, Nelson WJ, Theriot JA. Listeria monocytogenes exploits normal host cell processes to spread from cell to cell. J Cell Biol 1999;146(6):1333-1350.
16. Bucci C, Parton RG, Mather IH, Stunnenberg H, Simons K, Hoflack B, Zerial M. The small GTPase rab5 functions as a regulatory factor in the early endocytic pathway. Cell 1992;70(5):715-728.
17. Parashuraman S, Mukhopadhyay A. Assay and functional properties of SopE in the recruitment of Rab5 on Salmonella-containing phagosomes. Methods Enzymol 2005;403:295-309.
18. Alvarez-Dominguez C, Stahl PD. Increased expression of Rab5a correlates directly with accelerated maturation of Listeria monocytogenes phagosomes. J Biol Chem 1999;274(17):11459-11462.
19. Mukherjee K, Parashuraman S, Raje M, Mukhopadhyay A. SopE acts as an Rab5-specific nucleotide exchange factor and recruits non-prenylated Rab5 on Salmonella-containing phagosomes to promote fusion with early endosomes. J Biol Chem 2001;276(26):23607-23615.
20. Clemens DL, Lee BY, Horwitz MA. Deviant expression of Rab5 on phagosomes containing the intracellular pathogens Mycobacterium tuberculosis and Legionella pneumophila is associated with altered phagosomal fate. Infect Immun 2000;68(5):2671-2684.
21. Ravikumar B, Imarisio S, Sarkar S, O'Kane CJ, Rubinsztein DC. Rab5 modulates aggregation and toxicity of mutant huntingtin through macroautophagy

in cell and fly models of Huntington disease. J Cell Sci 2008;121(Pt 10):1649-1660.

22. Cataldo AM, Peterhoff CM, Troncoso JC, Gomez-Isla T, Hyman BT, Nixon RA. Endocytic pathway abnormalities precede amyloid beta deposition in sporadic Alzheimer's disease and Down syndrome: differential effects of APOE genotype and presenilin mutations. Am J Pathol 2000;157(1):277-286.

23. Seabra MC, Mules EH, Hume AN. Rab GTPases, intracellular traffic and disease. Trends Mol Med 2002;8(1):23-30.

24. Hutagalung AH, Novick PJ. Role of Rab GTPases in membrane traffic and cell physiology. Physiol Rev 2011;91(1):119-149.

25. Galperin E, Sorkin A. Visualization of Rab5 activity in living cells by FRET microscopy and influence of plasma-membrane-targeted Rab5 on clathrin-dependent endocytosis. J Cell Sci 2003;116(Pt 23):4799-4810.

26. Stenmark H, Vitale G, Ullrich O, Zerial M. Rabaptin-5 is a direct effector of the small GTPase Rab5 in endocytic membrane fusion. Cell 1995;83(3):423-432.

27. Kitano M, Nakaya M, Nakamura T, Nagata S, Matsuda M. Imaging of Rab5 activity identifies essential regulators for phagosome maturation. Nature 2008;453(7192):241-245.

28. Prada-Delgado A, Carrasco-Marin E, Pena-Macarro C, Del Cerro-Vadillo E, Fresno-Escudero M, Leyva-Cobian F, Alvarez-Dominguez C. Inhibition of Rab5a exchange activity is a key step for Listeria monocytogenes survival. Traffic 2005;6(3):252-265.

29. Henry RM, Hoppe AD, Joshi N, Swanson JA. The uniformity of phagosome maturation in macrophages. J Cell Biol 2004;164(2):185-194.

30. Alvarez-Dominguez C, Barbieri AM, Beron W, Wandinger-Ness A, Stahl PD. Phagocytosed live Listeria monocytogenes influences Rab5-regulated in vitro phagosome-endosome fusion. J Biol Chem 1996;271(23):13834-13843.

31. Ullrich O, Horiuchi H, Bucci C, Zerial M. Membrane association of Rab5 mediated by GDP-dissociation inhibitor and accompanied by GDP/GTP exchange. Nature 1994;368(6467):157-160.

32. Barker SL, Clark HA, Swallen SF, Kopelman R, Tsang AW, Swanson JA. Ratiometric and fluorescence-lifetime-based biosensors incorporating cytochrome c' and the detection of extra- and intracellular macrophage nitric oxide. Anal Chem 1999;71(9):1767-1772.

33. Hoppe A, Christensen K, Swanson JA. Fluorescence resonance energy transfer-based stoichiometry in living cells. Biophys J 2002;83(6):3652-3664.

34. Beemiller P, Hoppe AD, Swanson JA. A phosphatidylinositol-3-kinase-dependent signal transition regulates ARF1 and ARF6 during Fcgamma receptor-mediated phagocytosis. PLoS Biol 2006;4(6):e162.

35. Hoppe AD, Swanson JA. Cdc42, Rac1, and Rac2 display distinct patterns of activation during phagocytosis. Mol Biol Cell 2004;15(8):3509-3519.

36. Pizarro-Cerda J, Cossart P. Listeria monocytogenes membrane trafficking and lifestyle: the exception or the rule? Annu Rev Cell Dev Biol 2009;25:649-670.

37. Nielsen E, Cheung AY, Ueda T. The regulatory RAB and ARF GTPases for vesicular trafficking. Plant Physiol 2008;147(4):1516-1526.

38. van der Bliek AM. A sixth sense for Rab5. Nat Cell Biol 2005;7(6):548-550.

Chapter II

Coordination of the Rab5 Cycle on Macropinosomes

Abstract

The GTPase Rab5a regulates the homotypic and heterotypic fusion of membranous organelles during the early stages of endocytosis. Many of the molecules which regulate the Rab5a cycle of association with membranes, activation, deactivation and dissociation are known. However, the extent to which these molecular scale activities are coordinated on membranes to affect the behavior of individual organelles has not been determined. This study used novel Förster Resonance Energy Transfer (FRET) microscopic methods to analyze the Rab5a cycle on macropinosomes, which are large endocytic vesicles that form in ruffled regions of cell membranes. In Cos-7 cells and mouse macrophages stimulated with growth factors, Rab5a activation followed immediately after its recruitment to newly formed macropinosomes. Rab5a activity increased continuously and uniformly over macropinosome membranes then decreased continuously, with Rab5a deactivation preceding dissociation by 1-12 min. Although the maximal levels of Rab5a activity were independent of organelle size, Rab5a cycles were longer on larger macropinosomes, consistent with an integrative activity governing Rab5a dynamics on individual organelles. The Rab5a cycle was destabilized by microtubule depolymerization and by bafilomycin A1. Overexpression of activating and inhibitory proteins indicated that active Rab5a stabilized macropinosomes. Thus, overall Rab5a activity on macropinosomes is coordinated by macropinosome structure and physiology.

Introduction

Rab5 regulates the fusion, trafficking and recycling of early endosomes (1, 2). The Rab5 isoforms Rab5a, b and c are regulated by activating guanine nucleotide exchange factors (GEFs), inhibitory GTPase-activating proteins (GAPs) and proteins which facilitate Rab5 delivery to and removal from membranes (3). Rab5 functions in a multi-step cycle in which it associates with endosomal membranes in an inactive form, is activated by a GEF, and binds to effector proteins such as Rabaptin-5 (4), EEA1 (5), Rabankyrin-5 (6), Rabenosyn-5 (7) or the type III PI 3-kinase Vps34 (8). Rab5 is deactivated at the membrane by a GAP and then dissociates from the membrane as other Rab proteins increase their association. Membrane association is regulated by GDP-dissociation inhibitors (GDI) (9) and GDI-displacement factors (GDF) (10).

Despite consensus about the Rab5 cycle of membrane association and activation, the mechanisms which coordinate Rab5 dynamics on endocytic membranes remain largely unexplained. Rab5 GEFs and GAPs are regulated by proteins which are themselves regulated by other enzymes or by phosphatidylinositol 3-phosphate (PI3P) on vesicle membranes. Rab5 activation may involve positive feedback amplification through the Rab5 GEF Rabex-5 and the Rab5 effector Vps34, which synthesizes PI3P (11). Rab5 deactivation could result from GAP activities of other signaling proteins on endocytic vesicles; for example, p85α, the regulatory subunit of PI 3-kinase IA, is a Rab5 GAP (12). Rab5 deactivation occurs coordinately with the arrival of the late endosomal protein Rab7, through Rab7-dependent interference with Rabex-5 function (1, 13). However, it remains unknown how much individual Rab5 molecular cycles are coordinated with each other on any individual organelle and the extent to which organelle physiology or structure modulate Rab5 activity cycles.

Macropinosomes are large endocytic organelles which form in response to various stimuli. Some cells exhibit macropinocytosis spontaneously, while in other cells macropinocytosis is initiated by growth factors or membrane-permeabilizing peptides (14). Rab5 regulates macropinosome formation and

maturation (6, 15). As macropinosomes mature, they either recycle to the cell surface or lose Rab5 and acquire Rab7 before fusing with lysosomes (16, 17). The relationship between Rab5 activity and macropinosome dynamics is not known.

To analyze the regulation of the Rab5a cycle on macropinosomes, we developed a FRET microscopy system to visualize and quantify Rab5a cycle dynamics. Using fluorescent protein chimeras of Rab5a (CFP-Rab5a), the Rab5-binding domain from the amino terminus of EEA1 (YFP-RBD) and IRES vectors expressing monomeric Cherry (mCherry) and regulatory proteins, we measured the Rab5a cycle on individual macropinosomes. In Cos-7 cells stimulated with epidermal growth factor (EGF) and in murine bone marrow-derived macrophages (BMM) stimulated with macrophage colony-stimulating factor (M-CSF), quantitative fluorescence microscopy indicated that Rab5a association, activation, deactivation and dissociation occurred coordinately on individual macropinosomes. This coordination was disrupted by the microtubule depolymerizing drug nocodazole and by the proton ATPase inhibitor bafilomycin A1. Modulation of Rab5a cycling by coexpression of Rabex-5, Rin1, the GTPase-defective mutant CFP-Rab5a(S34N) or the GAP RabGAP-5 (18) indicated that active Rab5a stabilizes macropinosomes.

Materials and Methods

Tissue culture, Treatment and Transfection

The kidney fibroblast-like cell line Cos-7 (American Type Culture Collection) was maintained at 37°C with 5% CO_2. Cells were cultured in Dulbecco's Modified Eagle Medium (DMEM) supplemented with 10% heat-inactivated fetal bovine serum (HIFBS), 100 U/ml penicillin, 100 µg/mL and 4 mM L-glutamine (Invitrogen). Bone marrow-derived macrophages (BMM) were prepared from femurs of C57/BL6 mice and cultured 6 days, as described previously (19). For microscopy, Cos-7 cells were plated one day prior to imaging onto 25 mm, No. 1.5 circular coverslips (Fisher Scientific) at 2.0 x 10^5 cells per

coverslip. Cells were incubated for 4 hours to allow attachment to the coverslips, transfected with plasmids using Roche FuGENE HD, following the manufacturer's protocol (Roche Diagnostics) and serum-starved overnight prior to imaging. BMM were transfected using Mouse Macrophage Nucleofector kit (Lonza) according to the manufacturer's protocol, plated on coverslips and incubated in RPMI-1640 with 20% HIFBS, 4 mM L-glutamine, 20 U/ml penicillin and 20 µg/ml streptomycin for 3 hours. Cells were incubated for 20 hours in DMEM without added M-CSF.

For imaging, coverslips with cells were placed in a Leiden chamber (Harvard Apparatus) with Ringer's buffer (155 mM NaCl, 5 mM KCl, 2 mM $CaCl_2$, 1 mM $MgCl_2$, 2 mM NaH_2PO_4, 10 mM glucose, 10 mM HEPES at pH 7.2) at 37°C. Macropinocytosis was stimulated by addition of 100 ng/mL epidermal growth factor (EGF; R&D Systems) to Cos-7 cells, or 200 µg/mL macrophage colony-stimulating factor (M-CSF) to BMM. Bafilomycin A1 (0.5 µM, Sigma-Aldrich) and nocodazole (5 µM, Sigma-Aldrich) were added to Cos-7 cells 30 minutes prior to image acquisition.

Plasmids

Monomeric versions of the cyan fluorescent protein (CFP), citrine (YFP) and Cherry (mCherry) were used for all chimeric constructs (20). Rab5a, Rab5a(Q79L), Rab5a(S34N), Arf6(T27N), Cdc42(N17), Rac1(N17), RabGAP-5, Rin1 and Rabex-5 were cloned in YFP, CFP or mCherry vectors. RabGAP-5 plasmid was provided by F.A. Barr (Max-Planck Institute of Biochemistry, Martinsried, Germany). Constructs for Rin1 and Rabex-5 were provided by A.R. Saltiel (University of Michigan, Ann Arbor, Michigan). Polymerase chain reaction was used to amplify the Rab5-binding domain (RBD) from the amino terminus of EEA1 (residues 36-218 aa) which was subcloned into mCit-C1 and mCFP-C1 vectors (21-23). The Clontech pIRES2-EGFP vector was modified by replacing EGFP with mCherry. Rab5a, Arf6(T27N), Cdc42(N17), Rac1(N17), RabGAP-5, Rin1 and Rabex-5 were cloned into the pIRES2-mCherry using In-Fusion

Advantage PCR Cloning Kit (Clontech Laboratories Inc.). All constructs originated from human cDNA and all sequences of constructs were confirmed by DNA sequencing at the University of Michigan DNA Sequencing Core.

Ratiometric and Förster resonance energy transfer (FRET) microscopy

Cells were co-transfected with plasmids encoding YFP-RBD, CFP-Rab5a, mCherry or pIRES2-mCherry. The pIRES2 vector contains an internal ribosomal entry site (IRES) between its multiple cloning site and the fluorophore site which allows the translation of both in a single bicistronic mRNA. mCherry served as a cytosolic volume marker which corrected for optical pathlength due to cell shape. mCherry also allowed identification of cells expressing non-fluorescent Rab5-modifying proteins (GAPs and GEFs). Five images were acquired: Phase-contrast, I_A, which contains the FRET-independent fluorescence from the acceptor, I_D, which contains the fluorescence from the donor, I_F, which contains a mixture of donor, acceptor, and FRET fluorescence and I_R, which contains the fluorescence from mCherry. These images were acquired on a Nikon TE300 widefield inverted fluorescence microscope with a 60× 1.4 NA Planapo objective, excitation and emission filters in filter wheels, a temperature-controlled stage, shutters for both phase-contrast and epifluorescence and a cooled digital charge-coupled camera (Quantix; Photometrics, Tucson, AZ). The source of epifluorescent light was a mercury arc lamp (OSRAM GmbH, Augusburg, Germany). Images were corrected for exposure times and shade and bias corrections were applied before processing. All images were acquired using MetaMorph version 7.7r1 (Molecular Devices, Sunnyvale, CA).

FRET and ratiometric measurements were calculated for each cell using MATLAB R2009a (The Mathworks, Natick, MA), the DIPImage toolbox for MATLAB (http://www.diplib.org, Quantitative Imaging Group, Delft University of Technology, Netherlands) and FRET Calculator (available from the Center for Live Cell Imaging at the University of Michigan). Ratiometric images of YFP- and CFP-chimeras were calculated from three images, the YFP image I_A, the CFP

image I_D, and mCherry image I_R. The ratio of YFP- or CFP-chimera to mCherry reported the localization of each chimera normalized to cell volume. FRET stoichiometry (24) was used to measure the proportions of donor, acceptor and donor-acceptor complex in each pixel. FRET calibration parameters were determined using Cos-7 cells expressing YFP only (α), CFP only (β) or a linked YFP-CFP molecule of known FRET efficiency (γ and ξ). FRET Calculator was used to obtain the total concentrations of acceptor (A) and donor ($D = I_D + EDA*\xi$), the FRET efficiency times the concentration of donor-acceptor complex ($EDA = I_F - \alpha*I_A - \beta*I_D$), the fraction of the acceptor in complex times the FRET efficiency (E_A), the fraction of the donor in complex times the FRET efficiency (E_D), the average FRET efficiency ($E_{AVG} = (E_A+E_D)/2$), the ratio of acceptors to cytoplasmic marker (R_{YR}), the ratio of donors to cytoplasmic marker (R_{CR}) and molar ratio of acceptors to donors (R_M). The EO image was created by thresholding the E_{AVG} image with different binary masks made from D images. The masks were thresholded to identify only the CFP-Rab5a-positive organelles and a pseudocolor scale was applied to the masked E_{AVG} images, assigning different colors at 5% E_{AVG} steps (0 to 40% E_{AVG}), the new scaled images were overlayed onto the phase-contrast images (EO in Figs. 1, 3, 4C and 6). In Figures 4A, B and 5 the E_{AVG} images were thresholded with two different binaries from D images; the threshold was set to red for values from 0–8% and green from 8–40%. In figure 4C, the TO images were created by averaging the EDA images and subtracting the average noise from the original EDA images, the new EDA images were eroded and dilated in Metamorph to improve the visualization of the active Rab5a-positive tubules. The images were then overlaid as green on phase-contrast images.

Particle Tracking

The centroid-tracking algorithm TRACKOBJ of Metamorph was used to measure signals associated with macropinosomes, as previously described (24). Using the phase-contrast image, the center of the macropinosome was identified;

a region encompassing the macropinosome was drawn in the phase-contrast, E_A, E_D, EDA, E_{AVG}, A, D and Ratio images. To compare multiple image series, the macropinosome data traces were aligned by designating the first phase-contrast image containing a fully rounded macropinosome as the 1-min time point.

Data Analysis

To quantify the Rab5a activation cycle, the particle tracking plots for D (total Rab5a signal) and EDA (total FRET signal) images were selected and all values were normalized to the maximum and minimum values. D and EDA signals for each macropinosome were analyzed for the interval between half-maximal values ascending and descending (i.e., the width of the association or activation profiles). D and EDA signals were also analyzed to determine the intervals between D and EDA at half-maximal ascending and half-maximal descending parts of the curve (Fig. 2.2C). The mean E_{AVG}Max for each modulator was used to compare the effect on Rab5a FRET during macropinocytosis. To measure E_{AVG}Max and diameter on the unstable macropinosomes in RabGAP-5-expressing cells, the diameter of the circular ruffle was measured prior to collapse and fusion with the membrane.

Statistical analysis

A paired two-tailed Student's t-test (Two-Sample Assuming Equal Variances) was used to compare the effect on the E_{AVG}Max average of the macropinosomes formed in control cells, cells expressing pIRES2-mCherry-RabGAP-5, pIRES2-mCherry-Rin1 and cells expressing pIRES2-mCherry-Rabex-5.

Results

The Rab5a Cycle on Macropinosomes.

To analyze the Rab5a activation cycle on individual organelles, a widefield fluorescence microscopy system was designed for ratiometric and FRET microscopic analysis. Fluorescent chimeras of Rab5a and the amino terminal Rab5a-binding domain of EEA1 (RBD), which binds to GTP-Rab5a (21, 22), were developed and characterized. To study the activation cycle of Rab5a on macropinosomes, Cos-7 cells and murine BMM were transfected with plasmids encoding CFP-Rab5a, YFP-RBD and a pIRES2-mCherry vector. The mCherry reported cytoplasmic volume distribution and marked the cells expressing non-fluorescent proteins from pIRES2 transcripts. Macropinocytosis was stimulated by addition of EGF to serum-starved Cos-7 cells expressing fluorescent chimeras (25). The formation and intracellular movements of macropinosomes were observed by widefield phase-contrast and fluorescence microscopy (Fig. 2.1 A-D). FRET stoichiometry (24) was used to measure the essential parameters of Rab5a dynamics on macropinosomes. Informative parameters included D - the total fluorescence of CFP-Rab5a corrected for fluorescence loss due to FRET, EDA - the total fluorescence attributable to FRET and E_{AVG} - the average of the apparent donor and acceptor FRET efficiencies (Fig. 2.1E, F). By correcting for variations in the average ratios of CFP-Rab5a and YFP-RBD, E_{AVG} measures the level of Rab5a activation, with E_{AVG} of 0.40 approximating full activation. E_{AVG} images were thresholded using binary masks made from the D images (to identify CFP-Rab5a-positive organelles), then a pseudocolor scale was applied to the masked E_{AVG} images, assigning different colors at 5% E_{AVG} steps (0 to 40% E_{AVG}). Overlaying the masked, pseudocolored E_{AVG} images onto the phase-contrast images afforded study of the movements and activation patterns of CFP-Rab5a on individual macropinosomes (EO panels Fig. 2.1E). Cos-7 cells formed macropinosomes of various sizes, sometimes as large as 12 μm diameter (Fig. 2.1A-E). The levels of Rab5a activation varied between macropinosomes in a

single cell, but the FRET signal on each individual macropinosome was relatively uniform over the entire organelle, indicating signal integration at the organelle level. After reaching maximal EDA values, the FRET signals declined before the CFP-Rab5a dissociated from the macropinosome. Similar patterns of Rab5a dynamics were observed on macropinosomes in BMM stimulated with M-CSF (Fig. 2.1F).

The Rab5a overall activation cycle on macropinosomes was quantified and analyzed using algorithms developed in MetaMorph. CFP-Rab5a recruitment to macropinosomes increased gradually, reaching higher total levels on larger organelles (D, Fig. 2.2A). Similar patterns were observed for total levels of FRET (EDA, Fig. 2.2B). The cycle of Rab5a on each macropinosome was studied by normalizing curves to the maximal levels attained for D and EDA (Fig. 2.2C). The ascending curves for Rab5a association (D; CFP-Rab5a recruitment) and activation (EDA; YFP-RBD/CFP-Rab5a FRET) were nearly coincident, indicating that CFP-Rab5a was activated immediately as it associated with the macropinosome membrane. However, the EDA curve decreased sooner than the D curve, indicating that Rab5a was deactivated several minutes before it dissociated from the macropinosome.

Because macropinosomes form asynchronously after addition of growth factor (26), we could not use biochemical methods to measure rates of Rab5 activation on macropinosomes. Net Rab5 activation could be estimated by the rate of FRET increase on individual macropinosomes. The maximal rate of E_{AVG} increase was 0.033 per minute (± 0.003). However, this is not easily translated into a rate of Rab5 activation.

The relationships between macropinosome size and Rab5a cycle parameters were measured in several ways. Although macropinosome size in Cos-7 cells did not correlate with the maximal level of Rab5a activation (E_{AVG}Max, Fig. 2.2D), the duration of the Rab5a cycle increased with macropinosome size. By measuring cycle duration as the widths of the association and activation curves (parameters **a** and **b** of Fig. 2.2C), we determined that macropinosomes smaller than 3 μm diameter showed shorter

cycle times than did larger macropinosomes (Fig. 2.2E). Rab5a activation coincided with organelle association (parameter **c** of Fig. 2.2C), regardless of macropinosome size (solid symbols, Fig. 2.2F). However, on the descending curves, the EDA signal declined earlier than the D signal, indicating that Rab5a deactivation preceded Rab5a removal from the macropinosome membrane. The interval between Rab5a deactivation and dissociation increased with macropinosome size (open symbols, Fig. 2.2F). Macropinosomes formed by BMM were all less than 3 μm diameter. Although macropinosomes in BMM showed lower maximal E_{AVG} than similarly sized macropinosomes from Cos-7 cells (Fig. 2.2D), their overall Rab5a cycle dynamics were similar to macropinosomes of the same size in Cos-7 cells (Fig. 2.2E, F).

We quantified the extent to which probe expression altered Rab5 dynamics on macropinosomes. To examine the effects of YFP-RBD expression on the Rab5a association with macropinosomes, we compared Cos-7 cells expressing YFP-RBD, CFP-Rab5a and mCherry with Cos-7 cells expressing YFP-Rab5a and CFP. The presence of the YFP-RBD increased the rate of Rab5a association with macropinosomes. In cells expressing the FRET pair, the rate of change was 0.263 $\Delta R_M/R_C$ per minute (+/-0.09, n=5), whereas for cells expressing the YFP-Rab5a and CFP the rate was 0.293 $\Delta R_M/R_C$ per minute (+/-0.06, n=4). Moreover, expression of YFP-RBD prolonged the total Rab5a cycle. Without YFP-RBD, **a** = 3.67 min, with YFP-RBD, **a** = 17.75 min. This indicates that YFP-RBD enhanced Rab5 association with macropinosomes and inhibited dissociation. However, it remains possible that overexpression of FP-Rab5a accelerated Rab5 cycle dynamics on macropinosomes, but this could not be measured by our methods.

Rab5a activation cycle modulation by GEFs.

To modulate the Rab5a activation cycle, two GEFs were introduced into a pIRES2-mCherry vector and expressed in Cos-7 cells along with the Rab5a FRET reporter constructs. Use of the pIRES2 vectors expressing mCherry and

non-fluorescent GEFs allowed us to use mCherry fluorescence to identify cells expressing the non-fluorescent proteins. GEF effects on the Rab5a cycle were assessed by obtaining E_{AVG}Max for 15 macropinosomes (Fig. 2.3). In control macropinosomes expressing empty pIRES2-mCherry vector, E_{AVG}Max was 0.19 ± 0.018. Cos-7 cells expressing YFP-RBD, CFP-Rab5a and pIRES2-Cherry-Rabex-5 contained enlarged macropinosomes with significantly higher FRET values (E_{AVG}Max = 0.24 ± 0.014; $p < 0.001$). Cells expressing pIRES2-mCherry-Rin1 did not contain enlarged macropinosomes, but reached higher FRET levels than control macropinosomes (E_{AVG}Max = 0.32 ± 0.01; $p < 0.0001$). These were similar to levels observed after expression of constitutively active Rab5a (data not shown). Expression of Rabex-5 or Rin1 also increased the abundance of FRET-positive tubular extensions from macropinosomes (Fig. 2.3A, B). Thus, overexpression of Rab5a GEFs increased and prolonged Rab5a activity on macropinosomes and increased tubular endosome formation.

Bafilomycin A1 increases tubule formation and destabilizes the Rab5a cycle.

Inhibition of the proton ATPase by bafilomycin A1 inhibits acidification of endocytic compartments (27) and increases endosome tubulation (28). To examine the role of pH in the Rab5a cycle, Cos-7 cells transfected with YFP-RBD, CFP-Rab5a and mCherry were treated with bafilomycin A1 and stimulated with EGF. Bafilomycin A1 showed a range of effects on the Rab5a cycle. Macropinosomes showed increased active Rab5a on tubular endosomes protruding from macropinosomes near the center of the cell (Fig. 2.4C), suggesting that vacuolar pH affects Rab5-dependent tubule formation. The Rab5a cycle on macropinosomes was irregular. Compared to macropinosomes in control cells, which exhibited uniform cycles of Rab5 activation (Fig. 2.4 A, D-F), macropinosomes in bafilomycin A1-treated cells exhibited erratic patterns of Rab5a association and activation (Fig. 2.4B, G-I). FRET signals on macropinosomes had a variegated appearance (Fig. 2.4C). CFP-Rab5a association and dissociation sometimes occurred more than once on a

macropinosome and Rab5a association was not consistently accompanied by increased FRET (Fig. 2.4 G-I).

Microtubule depolymerization destabilizes the Rab5a cycle.

To examine whether microtubule-based motility affects the Rab5a cycle on macropinosomes, cells expressing YFP-RBD, CFP-Rab5a and mCherry were treated with the microtubule depolymerizing agent nocodazole. The few macropinosomes which did form in these cells did not contain tubular extensions, but like the bafilomycin A1-treated cells they showed irregular patterns of Rab5 activation (Fig. 2.5). FRET signals were uneven and sometimes not restricted to the macropinosome itself (Fig. 2.5A). This was also evident from the quantitative analysis (Fig. 2.5 B-E).

Inhibition of Rab5a activity destabilizes macropinosomes

To examine the roles of small GTPases in macropinosome formation and Rab5a activation, we expressed from pIRES2-mCherry vectors GTPase-deficient forms of small GTPases which affect motility and macropinocytosis, including Arf6(T27N), Cdc42(N17), Rac1(N17) and Rab5a(S34N), and measured their effects on macropinosome formation and the Rab5a cycle. Expression of pIRES2-mCherry constructs of Arf6(T27N), Cdc42(N17) and Rac1(N17) inhibited the cells' ability to ruffle and form macropinosomes (data not shown). In Cos-7 cells which were transfected with YFP-RBD, CFP-Rab5a(S34N) and pIRES2-mCherry and stimulated with EGF, no FRET was observed and the majority of macropinosomes that formed were unstable, fusing back with the membrane shortly after closure (Fig. 2.6A).

Expression of RabGAP-5 lowered FRET signals and destabilized macropinosomes.

Like cells expressing CFP-Rab5a(S34N), cells expressing Rab5a FRET reporters and pIRES2-mCherry-RabGAP-5 formed small macropinosomes with little CFP-Rab5a association and very low FRET signals (Fig. 2.6B). Many macropinosomes would start to form but fused back with the membrane. A small amount of CFP-Rab5a localized to these unstable macropinosomes, but E_{AVG}Max was very low (0.04 +/- 0.007, $p < 0.0001$, compared to controls). Macropinosome size and stability were measured in BMM expressing CFP and either YFP-Rab5a or YFP-Rab5a(S34N). YFP-Rab5a(S34N) decreased macropinosome size (Fig. 2.6C, D) and increased the fraction of unstable macropinosomes (Fig. 2.6E). Thus, the increase in unstable macropinosomes in Cos-7 and BMM expressing dnRab5a or RabGAP-5 indicated a role for Rab5a in stabilizing the macropinosome.

The effects of these overexpressed proteins on the Rab5a cycle in Cos-7 cells were analyzed relative to macropinosome size (Fig. 2.7). Macropinosomes in control cells were a wide range of sizes, all of which exhibited single cycles of Rab5a activation. Rabex-5 and Rin1 increased the overall levels of E_{AVG}Max. RabGAP-5 and Rab5a(S34N) showed low levels of Rab5a recruitment to nascent macropinosomes and little if any Rab5a activation. Bafilomycin A1 increased macropinosome size and Rab5a activity on tubular extensions. Although both bafilomycin A1 and nocodazole destabilized the Rab5a cycle on macropinosomes, neither significantly decreased overall FRET levels.

Thus, the analysis of Rab5a cycle dynamics on macropinosomes indicated novel mechanisms that regulate the level and overall uniformity of Rab5a activity on large areas of membrane.

Discussion

Using new tools to elucidate the dynamics of Rab5 in living cells, this study revealed a novel feature of organelle biology, which is that physiological parameters affect overall molecular cycles. These tools allowed us to observe and quantify the Rab5 cycle of association with macropinosomes, activation,

deactivation and dissociation. The ability to measure all of these parameters on individual organelles permitted analysis of the overall Rab5 cycle with respect to morphological transitions. Visualization of Rab5a dynamics revealed a single, continuous sequence of Rab5a localization, activation and deactivation covering the entire organelle. This indicated a large-scale coordination of Rab5 activity on macropinosomes. It is important to note that these methods measure net activities on organelles. Individual molecular cycles are likely more rapid.

The overall Rab5 cycle

Although expression of the fluorescent chimeras altered Rab5a dynamics, general patterns were evident. As the macropinosome formed, the D and EDA signals increased at the same rate, beginning just as the macropinosome closed into the cell. This indicated that the mechanisms of Rab5 association and activation are independent of the timing of growth factor addition (closure occurred at various times after EGF addition). The slope of E_{AVG} was not affected by the size of the macropinosome. Rab5 dissociation from the membrane occurred more slowly than deactivation. This delay was partly due to expression of YFP-RBD, which significantly slowed the Rab5a cycle, but it could also be the result of phosphoinositide turnover dynamics or delayed recruitment or access of Rab5-dissociation factors.

Size-dependent activities

Different sizes of macropinosomes showed similar overall patterns of Rab5 cycle dynamics. Small macropinosomes generally cycled faster than large macropinosomes. The principal size-dependent effect was on Rab5 dissociation from the macropinosome (Fig. 2.2F), which indicated a role for organelle size in maturation rates or Rab conversion (13). Movement of smaller endosomes around the forming macropinosome area suggested that mechanisms such as

piranhalysis (29) could play a role in reducing the cargo and diameter of the macropinosome to a size which can mature and fuse with the lysosomes.

Cycle modulation by GEFs and GAPs

The effects of Rab5 activity on macropinosome dynamics were analyzed by expressing GEFs and GAPs from mCherry-pIRES vectors. Overexpression of the GEFs Rabex-5 and Rin1 increased E_{AVG}Max values and the persistence of active Rab5a on macropinosomes. Sustained Rab5 association and activation on macropinosomes in these cells did not allow measurement of cycle times (i.e., D and EDA remained elevated). Interestingly, cells expressing Rabex-5 contained enlarged active Rab5a-positive vesicles that had formed prior to stimulation and image acquisition, a phenotype resembling the effect of overexpression of constitutively active Rab5a (data not shown). Rin1 overexpression did not result in enlarged endosomes, indicating that the two GEFs function in different aspects of macropinosome maturation. Both GEFs increased the number of active Rab5a-positive tubular endosomes, which appeared only rarely in control cells.
Conversely, cells expressing RabGAP-5 contained macropinosomes with low levels of FRET. Such cells also contained more cytosolic CFP-Rab5a, indicating a higher fraction of inactive Rab5a in those cells. Most macropinosomes were unstable. Typically, nascent macropinosomes would close into cells with an irregular profile, but would fail to mature into circular organelles. Rather, the irregularly shaped phase-bright organelles persisted for up to 2 minutes then collapsed, presumably by finally fusing with the plasma membrane. These unstable macropinosomes recruited little or no Rab5a and the Rab5a that did accumulate was inactive. Similar inhibition was observed in cells expressing YFP-RBD and CFP-Rab5a(S34N). BMM expressing YFP-Rab5a(S34N) and CFP increased the frequency of unstable macropinosomes when compared to BMM expressing YFP-Rab5a. These results indicate that activation of Rab5a plays a critical role in macropinosome stability. The failure of unstable macropinosomes to round up may be related to their ability to form tubular extensions. A study by

Kerr and Teasdale (30) showed that sorting nexins-1 and 5 (SNX1, SNX5) contribute to the formation of Rab5a-positive tubular extensions and the rounding of macropinosomes. Rab5a may facilitate the SNX-mediated tubulation necessary for macropinosome rounding.

Irregular Rab5a cycles

The uniformity of the Rab5a cycle on macropinosomes became more obvious with the appearance of irregular Rab5a cycles. Bafilomycin A1 treatment led to erratic cycles of Rab5a and irregular localization and activation of Rab5a on the macropinosome membrane. Treatment of cells with nocodazole also caused irregular and erratic patterns of Rab5a localization and activation on macropinosomes. Bafilomycin A1 and nocodazole did not affect the maximum levels of FRET on the macropinosomes (Fig. 2.7). These variegated patterns of Rab5a activation indicate the existence of signal integrating activities on organelle membranes and suggest that luminal pH and microtubule integrity affect overall cycle dynamics.

Tubular endosomes

Bafilomycin A1 increased the appearance of Rab5a-positive tubular endosomes that stretched from the nuclear area toward the edges of the cell and exhibited movements typical of microtubule-based motility. Conditions which caused sustained activation of Rab5a (Rin1 or Rabex-5) also created tubules with active Rab5a. Tubular endosome morphologies were shown by earlier studies to be microtubule-dependent (28). The increase in FRET-positive tubular endosomes after overexpression of Rabex-5 and Rin1 and after bafilomycin A1-treatment indicates a relationship between macropinosome pH, Rab5a activity and microtubule-based endosome trafficking. This could be attributable to the Rab5 effector Rabenosyn-5, which mediates microtubule-based extension of endosomal membranes (31).

Thus, imaging of Rab5a cycles on macropinosomes revealed the existence of mechanisms which shape the overall Rab5a cycle. We speculate that organelle size affects the rate of formation of 3’ phosphoinositides and concentrations of 3’ phosphoinositides affect overall levels of Rab5 GEF or GAP activities. Furthermore, these studies indicate that Rab5a activity facilitates the extension of tubules and the rounding of the macropinosome, which may help to stabilize the organelle.

Figure 2.1. Visualization of the Rab5a activation cycle on macropinosomes. (A) A Cos-7 cell transfected with CFP-Rab5a, YFP-RBD and mCherry, stimulated with EGF and viewed by phase-contrast microscopy (PC). The enlarged region shows a macropinosome labeled with CFP-Rab5a (B) and YFP-RBD (C), and the distribution of cytoplasm indicated by mCherry (D). (E) A time series showing a region of the cell shown in panels A-D, processed for ratiometric imaging of CFP-Rab5a ($D = I_D + EDA*\xi$) and for total fluorescence due to FRET between CFP-Rab5a and YFP-RBD ($EDA = IF - \alpha*I_A - \beta*I_D$). In the bottom row, E_{AVG} values are presented as pseudocolor overlaid on the phase-contrast images ($E_{AVG} = (E_A + E_D)/2$). Color scale indicates E_{AVG} values. EGF (100 ng/mL) was added after acquisition of the first frame. (F) BMM expressing CFP-Rab5a, YFP-RBD and mCherry, stimulated with M-CSF. Image processing for FRET stoichiometry obtained the CFP-Rab5a distribution (D), total FRET signal (EDA) and E_{AVG}. For both cells, CFP-Rab5a recruitment to macropinosomes coincided with the increase in FRET, but FRET decreased before CFP-Rab5a dissociated from the macropinosome. Scale bars = 10 μm.

Figure 2.1

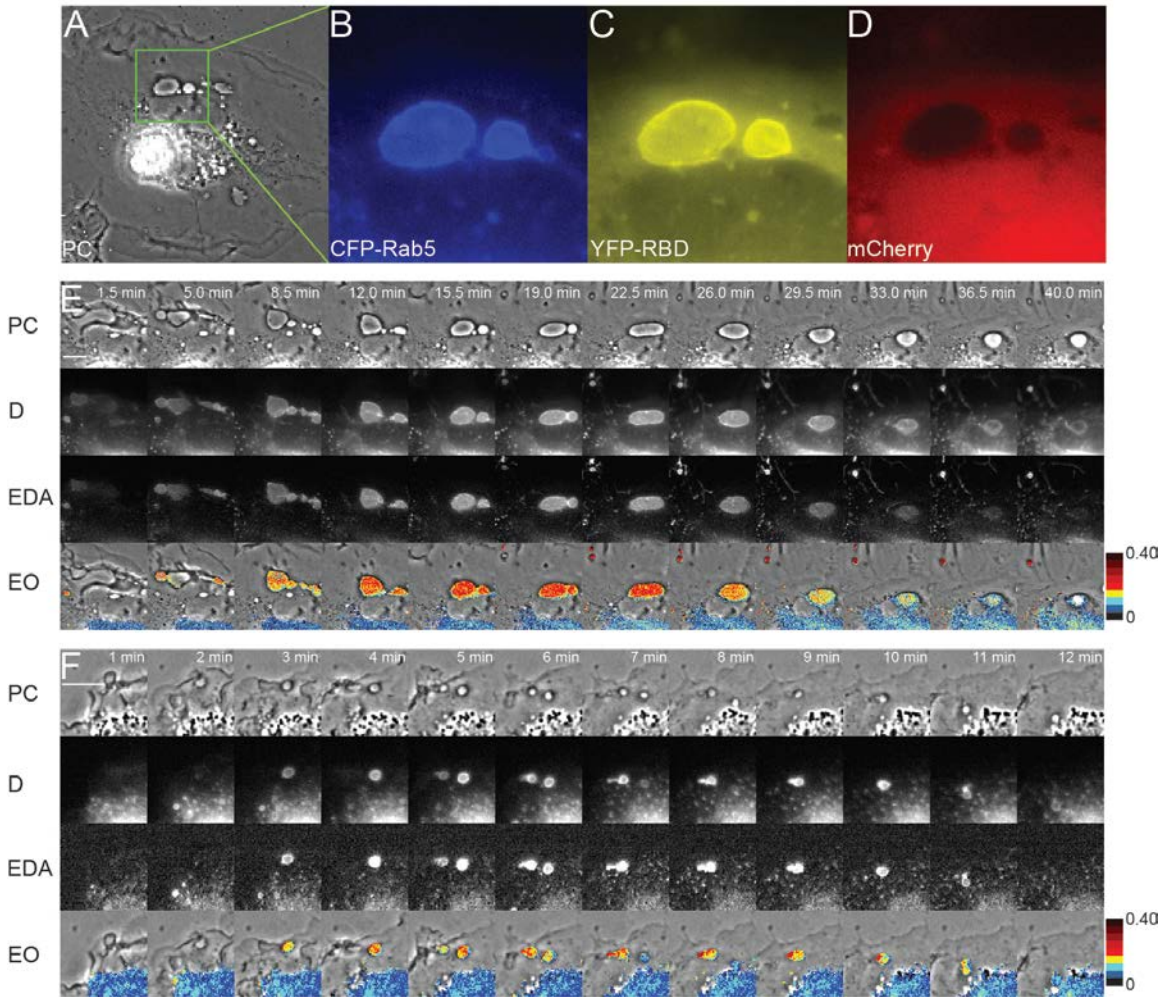
A
B
C
D
PC
CFP-Rab5
YFP-RBD
mCherry
E
1.5 min
5.0 min
8.5 min
12.0 min
15.5 min
19.0 min
22.5 min
26.0 min
29.5 min
33.0 min
36.5 min
40.0 min
PC
D
EDA
EO
0.40
0
F
1 min
2 min
3 min
4 min
5 min
6 min
7 min
8 min
9 min
10 min
11 min
12 min
PC
D
EDA
EO
0.40
0

Figure 2.2. The Rab5a cycle is slower on larger macropinosomes. (A-B) Quantification of the CFP-Rab5a activation cycle on individual macropinosomes of different diameters from Cos-7 cells, 7.5 μm (closed circles) and 2.2 μm (open circles). (A) CFP-Rab5a association and dissociation from macropinosomes. The larger macropinosome in the Cos-7 cell was labeled longer with CFP-Rab5a. (B) FRET from macropinosome-associated CFP-Rab5a and YFP-RBD (EDA). (C) Comparison of CFP-Rab5a association (closed symbols, from panel A) and activation (open symbols, from panel B) profiles on a single macropinosome from Cos-7 cells, normalized to the maximum and minimum values and plotted as Fraction of the Maximal Signal versus Time. Measured parameters were: **a**, for CFP-Rab5a association (D), the interval between the time the macropinosome reached half-maximal value ascending to the time it reached half-maximal value descending; **b**, for CFP-YFP FRET signals (EDA), the interval between the time the macropinosome reached half-maximal value ascending to the time it reached half-maximal value descending; **c**, for the ascending phase of D and EDA curves, the interval between the time of half-maximal D and half-maximal EDA; **d**, for the descending phases of the D and EDA curves, the interval between the time of half-maximal D and half-maximal EDA. (D) Maximal FRET signals (E_{AVG}Max) on individual macropinosomes, plotted vs. macropinosome diameter. Although maximal FRET signals were lower in BMM (triangles) than in Cos-7 cells (circles) for macropinosomes of comparable sizes, maximal FRET signals did not correlate with macropinosome size. (E) Half-maximal widths for Rab5a cycles were measured in macropinosomes of Cos-7 cells (circles) and BMM (triangles). CFP-Rab5a FRET cycles (a, closed symbols) were shorter than CFP-Rab5a association cycles (b, open symbols). Cycles were generally longer on larger macropinosomes. (F) For both Cos-7 cells (circles) and BMM (triangles), CFP-Rab5a activation coincided with association for all sizes of macropinosomes (c, closed symbols), whereas deactivation preceded dissociation by up to 12 min, with larger macropinosomes exhibiting longer lag times (d, open symbols).

Figure 2.2

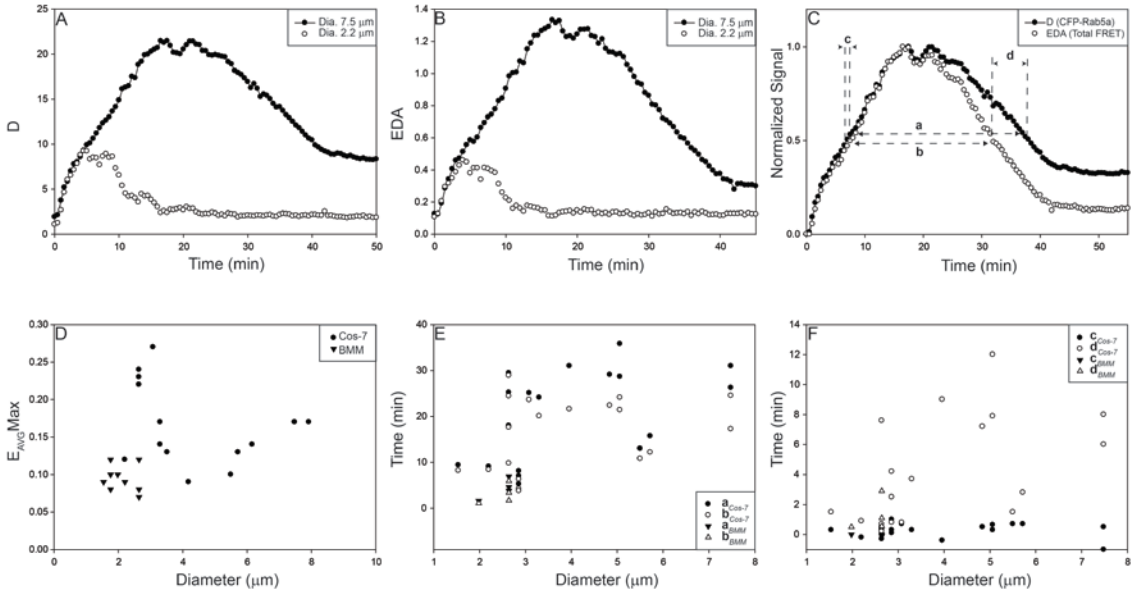
A
Dia. 7.5 μm
Dia. 2.2 μm
D
Time (min)
B
Dia. 7.5 μm
Dia. 2.2 μm
EDA
Time (min)
C
D (CFP-Rab5a)
EDA (Total FRET)
Normalized Signal
Time (min)
D
Cos-7
BMM
Diameter (μm)
E
Time (min)
Diameter (μm)
F
Time (min)
Diameter (μm)

Figure 2.3. Rab5a GEFs increase formation of macropinosome-associated tubules. (A) Cos-7 cell expressing FRET probes and pIRES2-mCherry-Rabex-5. (B) Cos-7 cell expressing FRET probes and pIRES2-mCherry-Rin1. Top row, phase-contrast; middle row, D (CFP-Rab5a); bottom row, EO (E_{AVG} Overlay). Overexpression of both GEFs increased CFP-Rab5a FRET on macropinosomes and remained higher than control. Macropinosomes extended tubules with high FRET signals. Color scale indicates E_{AVG} FRET signals. Scale bar = 10 μm.

Figure 2.3

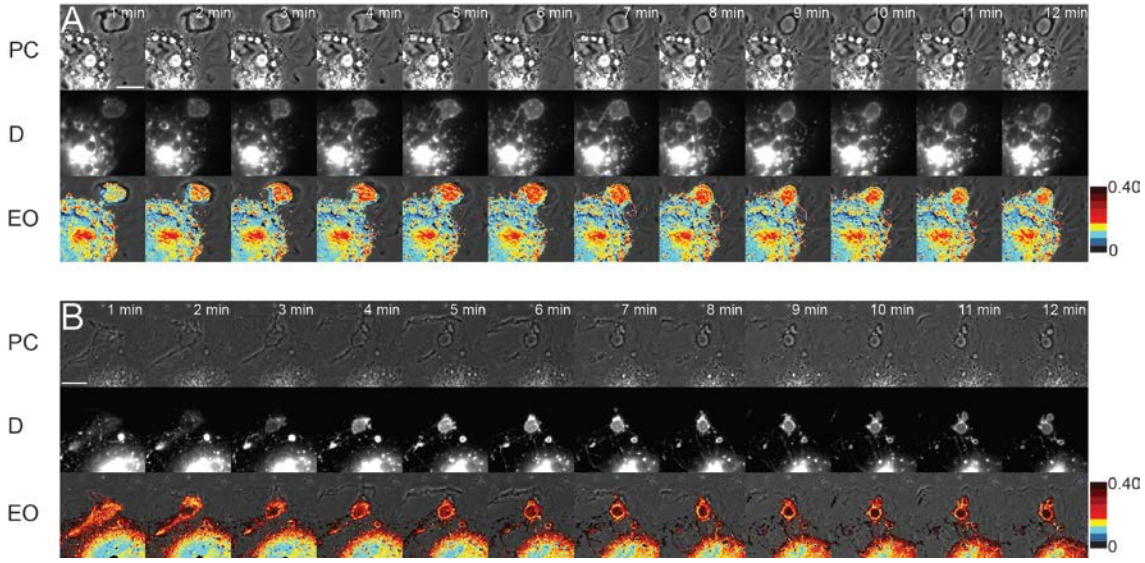
A
1 min
2 min
3 min
4 min
5 min
6 min
7 min
8 min
9 min
10 min
11 min
12 min
PC
D
EO
0.40
0
B
1 min
2 min
3 min
4 min
5 min
6 min
7 min
8 min
9 min
10 min
11 min
12 min
PC
D
EO
0.40
0

Figure 2.4. Bafilomycin A1 increases tubule formation and destabilizes the Rab5a cycle on macropinosomes. Macropinosomes in control cells (A) showed a single cycle of Rab5a activation and deactivation, whereas bafilomycin A1-treated cells (B) showed erratic patterns of CFP-Rab5a association, activation and deactivation and multiple tubular extensions with high Rab5a activity. Top row, phase-contrast; middle row, D (CFP-Rab5a); bottom row, EO [phase-contrast with overlay showing inactive CFP-Rab5a (red) and active CFP-Rab5a (green)], with the threshold for CFP-Rab5a activation set at E_{AVG} = 8%. (C) Top row, phase-contrast; middle row, TO, phase-contrast with overlay showing active Rab5 on tubular extensions (green) of cell treated with bafilomycin A1; bottom row; EO, E_{AVG} values presented as pseudocolor overlaid on phase-contrast. Scale bars = 10 μm. (D-I) Individual traces from macropinosomes in control (D-F) and bafilomycin A1-treated (G-I) Cos-7 cells showing CFP-Rab5 association (closed circles) and CFP-Rab5 FRET signals (open circles).

Figure 2.4

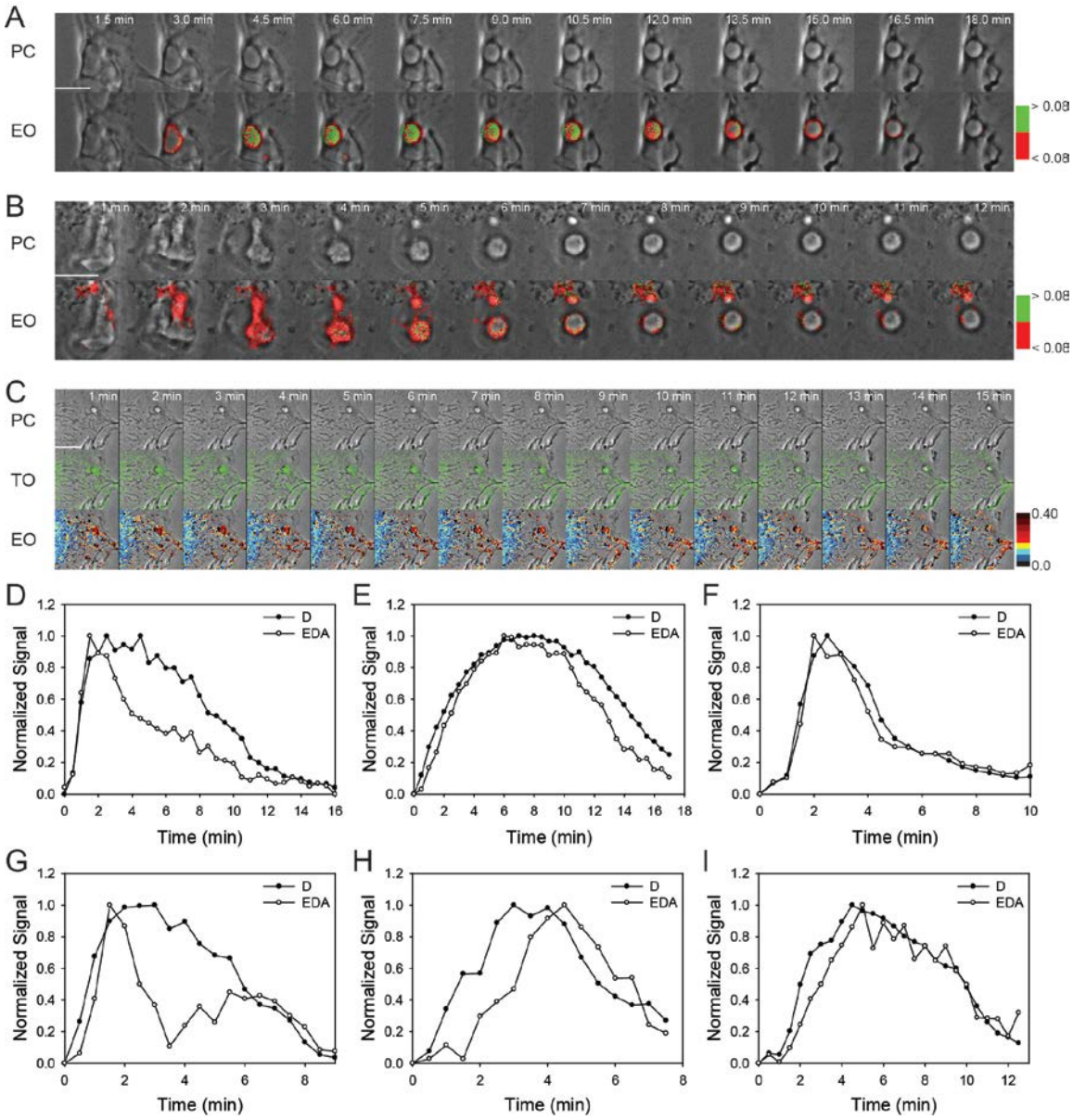
A
PC
EO
1.5 min
3.0 min
4.5 min
6.0 min
7.5 min
9.0 min
10.5 min
12.0 min
13.5 min
15.0 min
16.5 min
18.0 min
B
PC
EO
1 min
2 min
3 min
4 min
5 min
6 min
7 min
8 min
9 min
10 min
11 min
12 min
C
PC
TO
EO
1 min
2 min
3 min
4 min
5 min
6 min
7 min
8 min
9 min
10 min
11 min
12 min
13 min
14 min
15 min
0.40
0.0
D
E
F
G
H
I
Normalized Signal
Time (min)
D
EDA

Figure 2.5. Nocodazole destabilizes the Rab5a cycle on macropinosomes. (A) Rab5a activation on a macropinosome of a cell in nocodazole; top, phase-contrast; bottom, EO, phase-contrast with overlay showing inactive CFP-Rab5a (red) and active CFP-Rab5a (green), with the threshold for CFP-Rab5a activation set at E_{AVG} = 10%. Rab5a activity fluctuates on the macropinosome. Scale bar = 5 μm. (B-E) Individual traces from macropinosomes in nocodazole-treated cells.

Figure 2.5

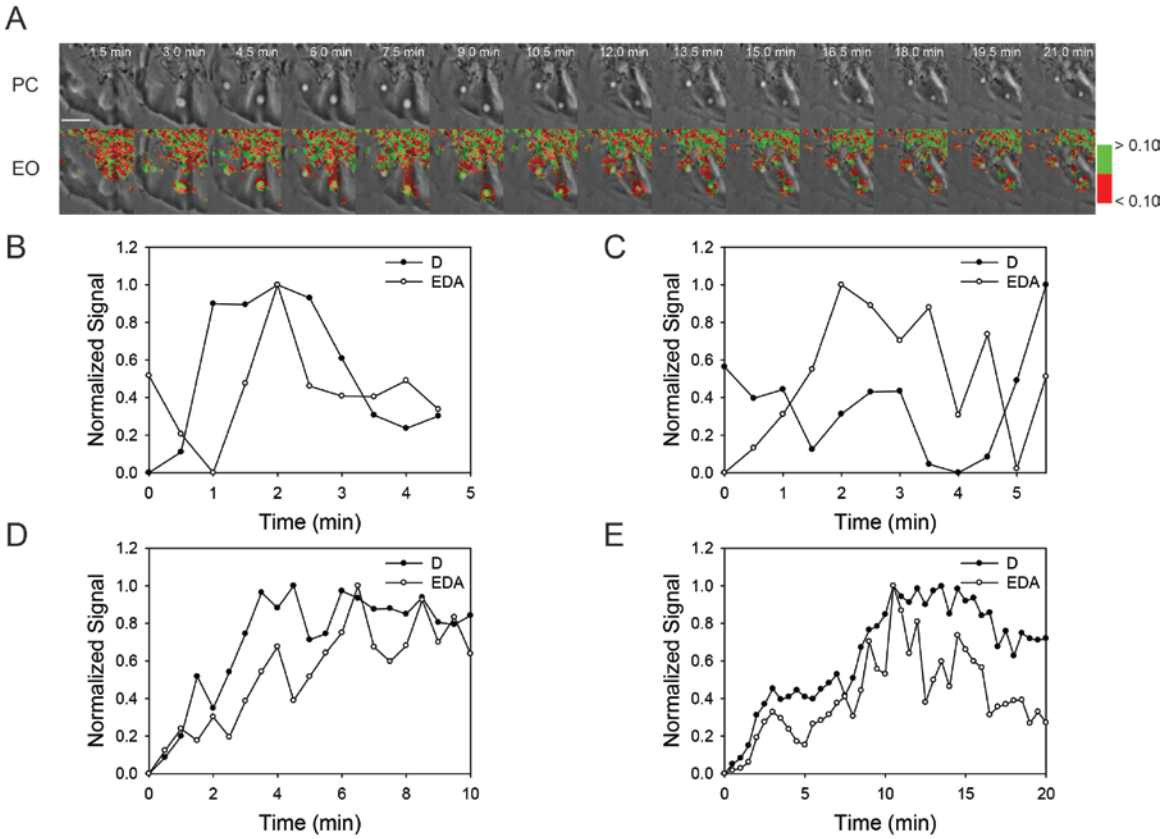
A
1.5 min
3.0 min
4.5 min
6.0 min
7.5 min
9.0 min
10.5 min
12.0 min
13.5 min
15.0 min
16.5 min
18.0 min
19.5 min
21.0 min
PC
EO
> 0.10
< 0.10
B
C
D
E
Normalized Signal
Time (min)
D
EDA

Figure 2.6. RabGAP-5 and Rab5a(S34N) destabilize macropinosomes. A) Cos-7 cells expressing YFP-RBD, CFP-Rab5a(S34N) and mCherry were stimulated by addition of EGF after the first frame was acquired. Small macropinosomes formed rarely. Most macropinosomes showed no association with CFP-Rab5a(S34N), no FRET and did not persist. B) Cos-7 cells expressing YFP-RBD, CFP-Rab5a and pIRES2-mCherry-RabGAP-5 formed macropinosomes, which showed low CFP-Rab5 association and low FRET signals. The vast majority of the macropinosomes were unstable and fused back with the membrane. Some small macropinosomes that were able to form showed low FRET signals. C, D) Macrophages expressing CFP-Rab5a(S34N) (black bars) formed smaller macropinosomes in response to M-CSF than macrophages expressing CFP-Rab5a (white bars). E) Macrophages expressing CFP-Rab5a(S34N) formed unstable macropinosomes more often than did macrophages expressing CFP-Rab5a.

Figure 2.6

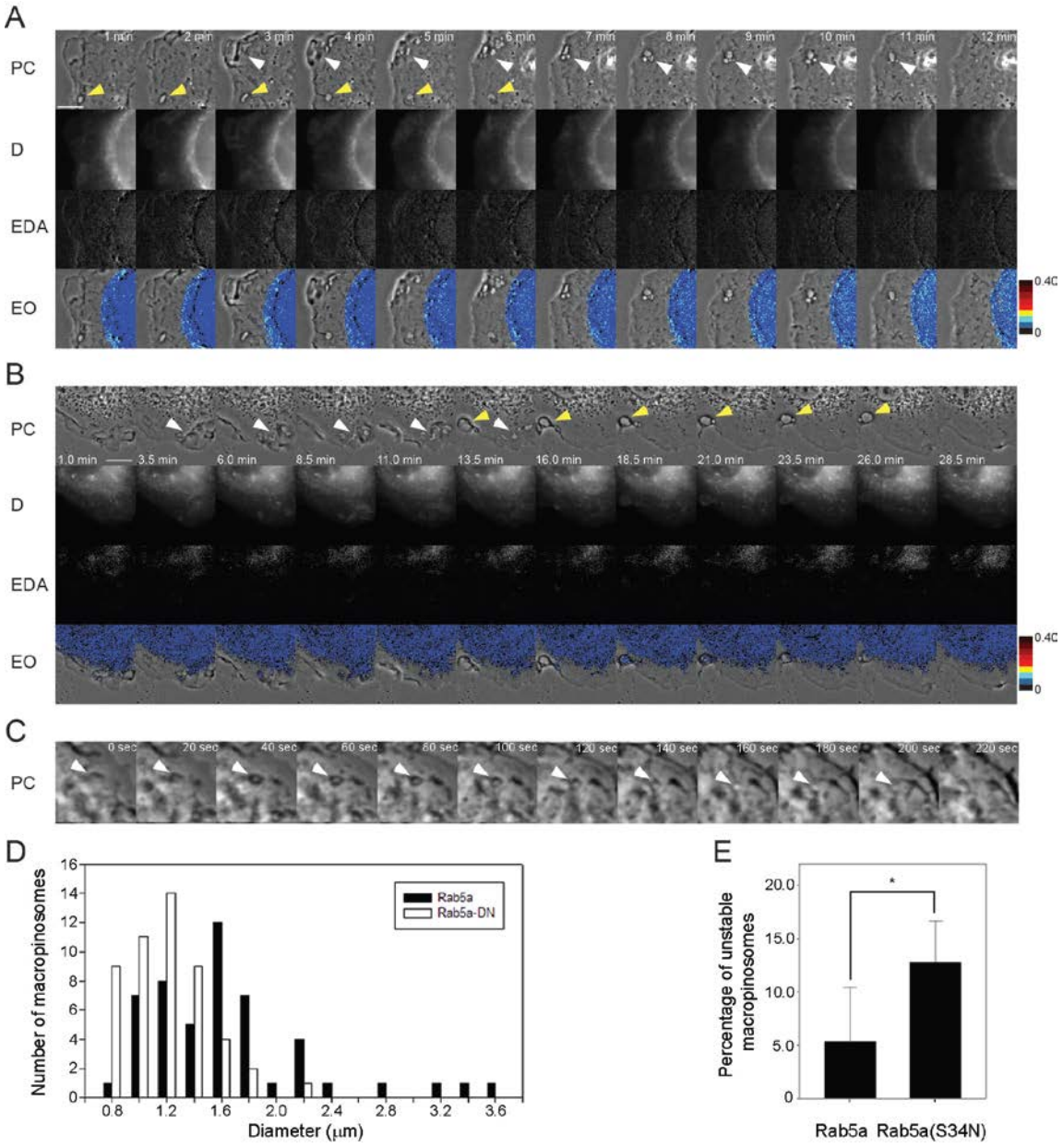
A
PC
D
EDA
EO
1 min
2 min
3 min
4 min
5 min
6 min
7 min
8 min
9 min
10 min
11 min
12 min
0.40
0
B
PC
D
EDA
EO
1.0 min
3.5 min
6.0 min
8.5 min
11.0 min
13.5 min
16.0 min
18.5 min
21.0 min
23.5 min
26.0 min
28.5 min
0.40
0
C
PC
0 sec
20 sec
40 sec
60 sec
80 sec
100 sec
120 sec
140 sec
160 sec
180 sec
200 sec
220 sec
D
Number of macropinosomes
Rab5a
Rab5a-DN
Diameter (μm)
E
Percentage of unstable macropinosomes
Rab5a
Rab5a(S34N)

Figure 2.7. The Rab5a cycle is modulated by GEFs and GAPs. Cos-7 cells were transfected with YFP-RBD, CFP-Rab5a and pIRES2-mCherry co-expressing GEFs (Rin1 and Rabex-5), GAP (RabGAP-5) or nothing (control). Cells were stimulated and macropinosomes were imaged and analyzed as in Figures 1 and 2. For each condition, the maximum E_{AVG} values were calculated for >9 macropinosomes and plotted as functions of macropinosome diameter. Relative to control cells expressing YFP-RBD, CFP-Rab5a and mCherry only, the GEFs, Rabex-5 and Rin1, increased E_{AVG}Max, whereas the GAP, RabGAP-5, decreased E_{AVG}Max. Treatment of control cells with bafilomycin A1 or nocodazole showed lower E_{AVG}Max levels, but these were not significant.

Figure 2.7

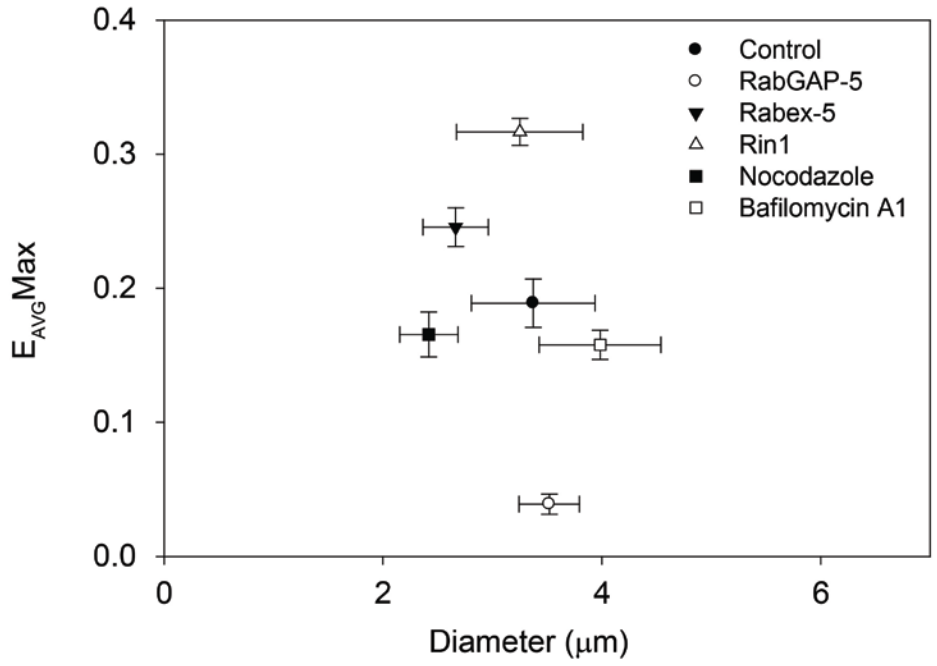
0.4
0.3
0.2
0.1
0.0
E_{AVG}Max
0
2
4
6
Diameter (μm)
Control
RabGAP-5
Rabex-5
Rin1
Nocodazole
Bafilomycin A1

Bibliography

1. Rink J, Ghigo E, Kalaidzidis Y, Zerial M. Rab conversion as a mechanism of progression from early to late endosomes. Cell 2005;122(5):735-749.

2. Perskvist N, Roberg K, Kulyte A, Stendahl O. Rab5a GTPase regulates fusion between pathogen-containing phagosomes and cytoplasmic organelles in human neutrophils. J Cell Sci 2002;115(Pt 6):1321-1330.

3. Bucci C, Lutcke A, Steele-Mortimer O, Olkkonen VM, Dupree P, Chiariello M, Bruni CB, Simons K, Zerial M. Co-operative regulation of endocytosis by three Rab5 isoforms. FEBS Lett 1995;366(1):65-71.

4. Stenmark H, Vitale G, Ullrich O, Zerial M. Rabaptin-5 is a direct effector of the small GTPase Rab5 in endocytic membrane fusion. Cell 1995;83(3):423-432.

5. Mu FT, Callaghan JM, Steele-Mortimer O, Stenmark H, Parton RG, Campbell PL, McCluskey J, Yeo JP, Tock EP, Toh BH. EEA1, an early endosome-associated protein. EEA1 is a conserved alpha-helical peripheral membrane protein flanked by cysteine "fingers" and contains a calmodulin-binding IQ motif. J Biol Chem 1995;270(22):13503-13511.

6. Schnatwinkel C, Christoforidis S, Lindsay MR, Uttenweiler-Joseph S, Wilm M, Parton RG, Zerial M. The Rab5 effector Rabankyrin-5 regulates and coordinates different endocytic mechanisms. PLoS Biol 2004;2(9):E261.

7. Nielsen E, Christoforidis S, Uttenweiler-Joseph S, Miaczynska M, Dewitte F, Wilm M, Hoflack B, Zerial M. Rabenosyn-5, a novel Rab5 effector, is complexed with hVPS45 and recruited to endosomes through a FYVE finger domain. J Cell Biol 2000;151(3):601-612.

8. Anderson DH, Chamberlain MD. Assay and stimulation of the Rab5 GTPase by the p85 alpha subunit of phosphatidylinositol 3-kinase. Methods Enzymol 2005;403:552-561.

9. Ullrich O, Stenmark H, Alexandrov K, Huber LA, Kaibuchi K, Sasaki T, Takai Y, Zerial M. Rab GDP dissociation inhibitor as a general regulator for the membrane association of rab proteins. J Biol Chem 1993;268(24):18143-18150.

10. Dirac-Svejstrup AB, Sumizawa T, Pfeffer SR. Identification of a GDI displacement factor that releases endosomal Rab GTPases from Rab-GDI. Embo J 1997;16(3):465-472.

11. Christoforidis S, Miaczynska M, Ashman K, Wilm M, Zhao L, Yip SC, Waterfield MD, Backer JM, Zerial M. Phosphatidylinositol-3-OH kinases are Rab5 effectors. Nat Cell Biol 1999;1(4):249-252.

12. Chamberlain MD, Berry TR, Pastor MC, Anderson DH. The p85alpha subunit of phosphatidylinositol 3'-kinase binds to and stimulates the GTPase activity of Rab proteins. J Biol Chem 2004;279(47):48607-48614.

13. Poteryaev D, Datta S, Ackema K, Zerial M, Spang A. Identification of the switch in early-to-late endosome transition. Cell 2010;141(3):497-508.

14. Swanson JA, Watts C. Macropinocytosis. Trends Cell Biol 1995;5(11):424-428.

15. Lanzetti L, Palamidessi A, Areces L, Scita G, Di Fiore PP. Rab5 is a signalling GTPase involved in actin remodelling by receptor tyrosine kinases. Nature 2004;429(6989):309-314.

16. Racoosin EL, Swanson JA. Macropinosome maturation and fusion with tubular lysosomes in macrophages. J Cell Biol 1993;121(5):1011-1020.

17. Hewlett LJ, Prescott AR, Watts C. The coated pit and macropinocytic pathways serve distinct endosome populations. J Cell Biol 1994;124(5):689-703.

18. Haas AK, Fuchs E, Kopajtich R, Barr FA. A GTPase-activating protein controls Rab5 function in endocytic trafficking. Nat Cell Biol 2005;7(9):887-893.

19. Henry RM, Hoppe AD, Joshi N, Swanson JA. The uniformity of phagosome maturation in macrophages. J Cell Biol 2004;164(2):185-194.

20. Kitano M, Nakaya M, Nakamura T, Nagata S, Matsuda M. Imaging of Rab5 activity identifies essential regulators for phagosome maturation. Nature 2008;453(7192):241-245.

21. Galperin E, Sorkin A. Visualization of Rab5 activity in living cells by FRET microscopy and influence of plasma-membrane-targeted Rab5 on clathrin-dependent endocytosis. J Cell Sci 2003;116(Pt 23):4799-4810.

22. Stenmark H, Aasland R, Toh BH, D'Arrigo A. Endosomal localization of the autoantigen EEA1 is mediated by a zinc-binding FYVE finger. J Biol Chem 1996;271(39):24048-24054.

23. Mishra A, Eathiraj S, Corvera S, Lambright DG. Structural basis for Rab GTPase recognition and endosome tethering by the C2H2 zinc finger of Early Endosomal Autoantigen 1 (EEA1). Proc Natl Acad Sci U S A 2010;107(24):10866-10871.

24. Hoppe A, Christensen K, Swanson JA. Fluorescence resonance energy transfer-based stoichiometry in living cells. Biophys J 2002;83(6):3652-3664.

25. Collins VP. The fine structure of growing and non-growing whole glia cell preparations. Cytobiologie 1978;18(2):327-338.

26. Yoshida S, Hoppe AD, Araki N, Swanson JA. Sequential signaling in plasma-membrane domains during macropinosome formation in macrophages. J Cell Sci 2009;122(Pt 18):3250-3261.

27. Yoshimori T, Yamamoto A, Moriyama Y, Futai M, Tashiro Y. Bafilomycin A1, a specific inhibitor of vacuolar-type H(+)-ATPase, inhibits acidification and protein degradation in lysosomes of cultured cells. J Biol Chem 1991;266(26):17707-17712.

28. D'Arrigo A, Bucci C, Toh BH, Stenmark H. Microtubules are involved in bafilomycin A1-induced tubulation and Rab5-dependent vacuolation of early endosomes. Eur J Cell Biol 1997;72(2):95-103.

29. Willingham MC, Yamada SS. A mechanism for the destruction of pinosomes in cultured fibroblasts. Piranhalysis. J Cell Biol 1978;78(2):480-487.

30. Kerr MC, Lindsay MR, Luetterforst R, Hamilton N, Simpson F, Parton RG, Gleeson PA, Teasdale RD. Visualisation of macropinosome maturation by the recruitment of sorting nexins. J Cell Sci 2006;119(Pt 19):3967-3980.

31. Nielsen E, Severin F, Backer JM, Hyman AA, Zerial M. Rab5 regulates motility of early endosomes on microtubules. Nat Cell Biol 1999;1(6):376-382.

Chapter III

Coordination and Regulation of Small GTPases during Macropinocytosis and Phagocytosis

Abstract

Infection of cells with *Listeria monocytogenes* (*Lm*) involves escape from its phagocytic vacuole prior to fusion with the lysosome. The small GTPase Rab5 limits the ability of *Lm* to escape from its compartment. *Lm* is able to modulate Rab5 activity, promoting GDP exchange of Rab5 (1). However, although Rab5 localizes to *Lm*-containing vacuoles in CHO cells and J774E cells, it does not localized to *Lm* vacuoles in RAW 264.7 macrophages (2, 3). To compare the dynamics of small GTPases during phagocytosis and *Lm* infection, we used Förster Resonance Energy Transfer (FRET) microscopic methods to measure Cdc42, Rac1, Rac2 and Rab5 activity during IgG-opsonized red blood cells (RBC) and *Lm* uptake in murine primary bone marrow-derived macrophages. During RBC phagocytosis, Rac1 and Rac2 localized to the phagosome and Cdc42 was localized to the leading edge of the phagocytic cup. Rab5 localized to the phagosome but showed low levels of activity. During *Lm* uptake, all four GTPases showed activation. Rac1 was activated on a subset of *Lm*-containing vacuoles. Rab5 showed varying levels of activation on *Lm*-containing vacuoles. Rab5 activity was higher on macropinosomes that formed in the vicinity of phagocytic events than on RBC phagosomes or *Lm*-containing vacuoles. During uptake of hemolysin-deficient or heat-killed *Lm*, Rab5 localized to the vacuole with low levels of FRET, suggesting a possible role of LLO in the activation of Rab5. During vesicle fusion events, Rab5 activity was higher at the

point of contact between both vacuoles. Moreover, during vesicle fusion Rab5 activity increased over the entire organelle, starting at the point of contact and radiating around the new vacuole. These studies indicate that *Lm* modulates the activities of small GTPases, particularly Rab5, during infection of macrophages.

Introduction

Endocytosis comprises a group of mechanisms by which cells obtain nutrients from the environment and internalize particles or pathogens. Two endocytotic mechanisms are macropinocytosis and phagocytosis. Macropinocytosis allows cells to internalize relatively large amounts of extracellular fluids, which may be used to obtain nutrients or to sample the environment for immune surveillance. Phagocytosis is the engulfment by cells of particles or pathogens. It is commonly used by innate immune cells such as macrophages to kill microbes. Both mechanisms require the extension of actin-rich membrane ruffles which close by fusing at their distal margins, creating macropinosomes or phagosomes as intracellular vacuoles. These compartments usually fuse with early endosomes, then acidify and mature into compartments resembling late endosomes and lysosomes. These transitions are regulated by phosphoinositides and small GTPases. Recent studies have looked at the main proteins involved in both pathways and how each pathway differs in the recruitment, localization and activation of each protein. Among the small GTPases involved in phagocytosis, Cdc42, Rac1, Rac2 and Rab5 play major roles in the early stages of uptake. Cdc42, Rac1 and Rac2 organize actin cytoskeleton rearrangement that leads to the extension of the ruffle and formation of the vacuole. Work done by Yoshida, et al. (4), showed that during M-CSF-stimulated macropinocytosis in murine bone marrow-derived macrophages Rac1 but not Rac2 was involved in the formation of the macropinosome. Hoppe, et al. (5), showed that during phagocytosis of opsonized sheep RBC by macrophage-like RAW 264.7 cells both Rac1 and Rac2 localized to the forming phagosome. In both studies Cdc42 activity localized to the tip of

the extending ruffles. Rab5 has been shown to localize to both forming phagosomes and macropinosomes (4, 6).

Survival and replication inside neutrophils and macrophages is crucial for the virulence of microbes. Some pathogens have evolved mechanisms to interfere with crucial steps of phagocytosis, such as delay of phagosome fusion with the lysosome or escape from the phagosome into the cytoplasm. Studies have pointed toward the small GTPase, Rab5a, as a target of multiple pathogens. Rab5 is a member of the Rab family of small GTPase which are a subgroup of the Ras GTPase family. It regulates docking and fusion of endocytic vesicles with early endosomes as well as the homotypic fusion of early endosomes. Rab5 is also involved in the translocation and activation of Rac2, leading to the oxidative burst (7). Previous work in our laboratory, using fluorescent chimeras of Rab5a and ratiometric fluorescence microscopy, showed that the maturation pathway of phagosomes in macrophages follows a sequential appearance of actin, Rab5a, Rab7 and LAMP1. Other groups showed that the inhibition of Rab5a or Rab7 could alter the progression of phagosomes to lysosomes, indicating the importance of these proteins. The main two ways pathogens modulate Rab5 activity are: 1) by keeping Rab5 in its GTP-bound or active form, which promotes continuous fusion with early endosomes and delays phagosome maturation and 2) by keeping Rab5 in its GDP-bound or inactive form, thus abolishing all fusion events. Pathogens such as *Salmonella* have specific virulence factors that keep Rab5 on its active form (8), while *Mycobacterium tuberculosis* uses deactivation of Rab5 to delay degradation (9).A number of diseases, such as Alzheimer's, Huntington's and some types of cancers, are caused in part by disruption of Rab5 cycling (10-14).

The intracellular pathogen, *Listeria monocytogenes* (*Lm*), is a Gram-positive bacterium which is capable of avoiding degradation by escaping from the phagosome into the cytoplasm. *Listeria monocytogenes* arrests maturation of the *Lm*-containing vacuole. Previous studies have shown that overexpression of Rab5 in macrophages reduces intracellular survival of *Lm* after infection (15). Rab5 localization to the *Lm*-containing vacuole appears to vary with target cell

type. Rab5 might play an important role in *Lm* survival. *Lm* targets Rab5 via its virulence factor p40 protein, a glyceraldehyde-3-phosphate dehydrogenase (GAPDH) (1, 3, 16). This virulence factor keeps Rab5 in its inactive form and allows time for LLO to perforate vacuolar membranes. Alvarez-Dominguez, et al. (3), observed localization of Rab5 to *Lm*-containing vacuoles of J774E and CHO cells. In contrast, Henry, et al. (2), observed that Rab5 did not localize to the *Lm*-containing vacuoles in RAW264.7 cells. These latter studies suggest cell-specific differences in the role of Rab5 during *Lm* infections.

To test the hypothesis that *Lm* alters Rab5a activation on *Lm*-containing vacuoles, we compared the dynamics and activation patterns of Rab5a during macropinocytosis and phagocytosis of RBC or *Lm*. FRET and ratiometric fluorescence microscopy were used to study Rab5a activation patterns in murine bone marrow-derived macrophages co-transfected with probes of Rab5 activity, including the chimeras YFP-RBD and CFP-Rab5a. Co-expressing the fluorescent protein mCherry as a volume marker, we calculated YFP-RBD/Cherry and CFP-Rab5a/Cherry ratios as well as FRET between YFP-RBD and CFP-Rab5a. Activation of Rab5a on RBC-containing phagosomes was lower than the levels of activation on macropinosomes. Rab5 activities on *Lm*-containing vacuoles were lower than on macropinosomes. Rab5 activation levels were lower on vacuoles containing hemolysin-deficient (*hly*-) and heat-killed *Lm*-containing vacuoles than on vacuoles containing wild-type bacteria, indicating a possible effect of hemolysin on Rab5 activation. Thus, Rab5a localized to red cell phagosomes, *Lm*-containing vacuoles and macropinosomes, whereas Rab5a activation was reduced on red cell phagosomes and *Lm*-containing vacuoles relative to macropinosomes. Dynamic studies revealed that YFP-Rab5a was recruited with similar kinetics to both red blood cell-containing phagosomes and *Lm*-containing vacuoles. A YFP chimera of Rab5-binding domain from EEA1 (YFP-RBD), which binds to endogenous active Rab5a, showed similar Rab5a localization and activation on red cell phagosomes and *Lm*-containing vacuoles.

We also used FRET microscopy to measure Cdc42, Rac1 and Rac2 activation patterns during RBC and *Lm* uptake in BMM. All three showed patterns during RBC phagocytosis consistent with previous studies (6, 17). During *Lm* infection, Rac1 was activated in only a subset of vacuoles, which indicated that *Lm* may modulate Rac1 activity.

Methods and Materials

Tissue culture, Treatment and Transfection

Murine bone marrow-derived macrophages (BMM) were prepared from femurs of C57/BL6 mice purchased from Jackson Laboratories (Bar Harbor, ME, USA; Stock Number 000664) and cultured 6 days, as described previously (18). For microscopy, cells were transfected the day before imaging using Lonza's Amaxa Mouse Macrophage Nucleofector kit (Basel, Switzerland) according to the manufacturer's protocol, plated onto 25 mm, No. 1.5 circular coverslips (Fisher Scientific) at 1.0 x 10^6 cells per coverslip and incubated in RPMI-1640 with 20% HIFBS, 4 mM L-glutamine, 20 U/ml penicillin and 20 µg/ml streptomycin for 4 hours. After 4 hours cells were washed with 1X PBS (Gibco) and incubated in fresh RPMI-1640 overnight.

Red blood cell phagocytosis

For imaging, coverslips with cells were placed in a Leiden chamber (Harvard Apparatus) with 0.4 mL of Ringer's buffer (155 mM NaCl, 5 mM KCl, 2 mM CaCl, 1 mM MgCl, 2 mM NaH_2PO_4, 10 mM glucose, 10 mM HEPES at pH 7.2) at 37°C and maintained in a heated observation chamber at 37°C. After selection of a transfected cell, 10^5 IgG-opsonized erythrocytes (5 µL) were added to the coverslip. Image collection began as erythrocytes came into contact with the macrophage. Images were acquired at 30-sec intervals.

Bacterial strains and preparation

L. monocytogenes wild-type strain DP-L10403 and *hly*- deletion strain DP-L2161 were grown overnight at room temperature in brain heart infusion (BHI) broth. They were subcultured the next day and grown for 1 hour to an OD600 of 0.500 at 37°C. Sub-cultured bacteria (1 mL) were washed three times in Ringer's buffer (RB; 155 mM NaCl, 5 mM KCl, 2 mM $CaCl_2$, 1 mM $MgCl_2$, 2 mM NaH_2PO_4, 10 mM Hepes and 10 mM glucose, pH 7.2).

Listeria uptake

After selection of a transfected macrophage, 100 μL of the sub-cultured *Lm* were added to the coverslip and incubated for 2 minutes. Images were acquired at 30-sec intervals, beginning immediately after the 2-minute incubation.

Plasmids

Monomeric versions of the cyan fluorescent protein (CFP), citrine (YFP) and Cherry (mCherry) were used for all chimeric constructs (6). YFP constructs of RBD, Cdc42, Rac1 and Rac2 and CFP constructs of Rab5a and PBD were previously described (6). All sequences of constructs were confirmed by DNA sequencing at the University of Michigan DNA Sequencing Core.

Ratiometric and fluorescence resonance energy transfer (FRET) microscopy

Cells were co-transfected with plasmids encoding YFP, CFP chimeras of the GTPase and its correspondent binding domain and mCherry. mCherry served as a cytosolic volume marker which corrected for optical pathlength due to cell shape. Five images were acquired: Phase-contrast, I_A, which contains the FRET-independent fluorescence from the acceptor, I_D, which contains the fluorescence from the donor, I_F, which contains a mixture of donor, acceptor,

and FRET fluorescence and I_R, which contains the fluorescence from mCherry. These images were acquired on a Nikon TE300 widefield inverted fluorescence microscope with a 60× 1.4 NA Planapo objective, excitation and emission filters in filter wheels, a temperature-controlled stage, shutters for both phase-contrast and epifluorescence and a cooled digital charge-coupled camera (Quantix; Photometrics, Tucson, AZ). The source of epifluorescent light was a mercury arc lamp (OSRAM GmbH, Augusburg, Germany). Images were corrected for exposure times and shade and bias corrections were applied before processing. All images were acquired using MetaMorph version 7.7r1 (Molecular Devices, Sunnyvale, CA).

FRET and ratiometric microscopy measurements were calculated for each cell using MATLAB R2009a (The Mathworks, Natick, MA), the DIPImage toolbox for MATLAB (http://www.diplib.org/, Quantitative Imaging Group, Delft University of Technology, Netherlands) and FRET Calculator (available from the Center for Live Cell Imaging at the University of Michigan). Ratiometric images of YFP- and CFP-chimeras were calculated from three images, the YFP image I_A, the CFP image I_D, and mCherry image I_R. The ratio of YFP- or CFP-chimera to mCherry reported the localization of each chimera normalized to cell volume. FRET stoichiometry (5) was used to measure the proportions of donor, acceptor and donor-acceptor complex in each pixel. FRET calibration parameters were determined using Cos-7 cells expressing YFP only (α), CFP only (β) or a linked YFP-CFP molecule of known FRET efficiency (γ and ξ). FRET Calculator was used to obtain the total concentrations of acceptor (A) and donor ($D = I_D + EDA*\xi$), the FRET efficiency times the concentration of donor-acceptor complex ($EDA = I_F - \alpha*I_A - \beta*I_D$), the fraction of the acceptor in complex times the FRET efficiency (E_A), the fraction of the donor in complex times the FRET efficiency (E_D), the average FRET efficiency ($E_{AVG} = (E_A+E_D)/2$), the ratio of acceptors to cytoplasmic marker (R_{YR}), the ratio of donors to cytoplasmic marker (R_{CR}) and molar ratio of acceptors to donors (R_M). The EO image was created by thresholding the E_{AVG} image with different binary masks made from D images. The masks were thresholded to identify only the cargo-positive organelles and a

pseudocolor scale was applied to the masked E_{AVG} images, assigning the color red to E_{AVG} values below a specific cut-off and green for values above the cut-off, the new scaled images were overlayed onto the phase-contrast images. In Figures 3.1, 3.2 and 3.3, the overlay images display red to indicate regions containing inactive Rab5a and green where Rab5 activity is greater than some threshold value. The threshold values were selected to illustrate peaks of Rab5 activation relative to the morphology. On a scale of E_{AVG} values from 0 to 40%, the threshold values ranged from 6% (Fig. 3.3C, D) to 12% (Figs. 3.1C and 3.2D).

In Figure 3.4B, the EO image was created by thresholding the E_{AVG} image with different binary masks made from D images. The masks were thresholded to identify only the CFP-Rab5a-positive organelles and a pseudocolor scale was applied to the masked E_{AVG} images, assigning different colors at 5% E_{AVG} steps (0 to 40% E_{AVG}), the new scaled images were overlayed onto the phase-contrast images.

Particle Tracking

The centroid-tracking algorithm TRACKOBJ of Metamorph was used to measure signals associated with macropinosomes, as previously described (5)**.** Using the phase-contrast image, the center of the macropinosome was identified; a region encompassing the macropinosome was drawn in the phase-contrast, E_A, E_D, EDA, E_{AVG}, A, D and Ratio images. To compare multiple image series, the macropinosome data traces were aligned by designating the first phase-contrast image containing a fully rounded macropinosome as the 1-min time point.

Recruitment Index R_{MP}/R_C

A recruitment index was used to compare chimera recruitment to macropinosomes in cells expressing varying concentrations of two (YFP-chimera

and free CFP) or three (YFP- and CFP-chimeras and free mCherry) proteins. Free CFP or mCherry, presumably distributed in cytoplasm without selective binding, and reported the distribution of cytoplasm. Dividing the Ratio on the macropinosome or phagosome R_{MP} by the Ratio for the entire cell R_C obtained the relative concentration of each chimera on the macropinosome, as described below

$$R_{MP}/R_C = [YFP]_{MP}[CFP]_C/[YFP]_C[CFP]_{MP} = [YFP]_{MP}/[YFP]_C$$

or

$$R_{MP}/R_C = [YFP]_{MP}[mCherry]_C/[YFP]_C[mCherry]_{MP} = [YFP]_{MP}/[YFP]_C \text{ ;}$$

$$R_{MP}/R_C = [CFP]_{MP}[mCherry]_C/[CFP]_C[mCherry]_{MP} = [CFP]_{MP}/[CFP]_C$$

Results

Cdc42, Rac1 and Rac2 Activation Patterns during RBC Phagocytosis

To measure Rho-family GTPase activities during endocytosis, BMM were transfected with YFP chimeras of Cdc42, Rac1 or Rac2 and with CFP-PBD, the p21-binding domain from Pak1 which binds to active forms of all three GTPases. Cells were fed IgG-opsonized sheep RBCs. After binding of the RBC to the cell, image series were acquired at 30-second intervals. We observed that all three GTPases were activated in forming phagosomes; Cdc42 was at the leading edge of the extending ruffle and showed low levels of activation, peaking at an E_{AVG}Max of 0.10. Rac1, Rac2 and Rab5 localized to the forming phagosome, Rac1 first localized to the forming phagosome around 30 seconds before Rac2. Rac1 values reached an E_{AVG}Max of 0.15 and Rac2 values reached an E_{AVG}Max of 0.12.

Cdc42, Rac1 and Rac2 Activation Patterns during Lm uptake

Similar methods were used to measure the activation of Cdc42, Rac1 and Rac2 during *Lm* uptake. All three GTPases were recruited to the forming *Lm*-containing vacuole. Cdc42 activation peaked at an E_{AVG}Max of 0.10. Due to the size of the *Lm*-containing vacuole and the speed of the event, we were not able to discern if Cdc42 localized only to the leading edge of the ruffle, as it did during phagocytosis of RBC and during macropinocytosis. Rac2 also localized to the forming vacuole, reaching E_{AVG}Max values of 0.13. Interestingly Rac1 localization and activation were observed on only a subset of BMM. In those cases where Rac1 localized to the forming *Lm*-containing vacuole, it reached E_{AVG}Max levels of 0.19.

Differences in Rab5a activation levels during macropinocytosis and phagocytosis of RBC and L. monocytogenes

During phagocytosis of IgG-opsonized sheep RBCs, we observed Rab5a localization to the phagosome with relatively little Rab5a activation. To analyze Rab5a dynamics during *Lm* infection, BMM were transfected with YFP-RBD, the amino terminal Rab5-binding domain of EEA1, CFP-Rab5a and mCherry, which served as a volume marker and allowed ratiometric fluorescence microscopy. Transfected BMM were incubated with *Lm* for 2 minutes and images were acquired at 30-second intervals beginning immediately after incubation. Rab5a showed a diverse population within the same cell. The ratio of CFP-Rab5a to mCherry (RCR) indicated that Rab5a localized to the phagosome, but E_{AVG}Max was only 0.10. *Lm*-containing vacuoles had E_{AVG}Max levels ranging from 0.05 to 0.15 and most were in the lower part of the range. This was less than the E_{AVG}Max of Rab5a on the macropinosomes that formed nearby, which reached E_{AVG}Max values of 0.20. Heat-killed *Lm* and *hly- Lm*, a *Lm* mutant that does not express the pore forming cytolysin listeriolysin O (LLO), were also tested.

Surprisingly, neither of them showed high levels of Rab5a FRET; the mean E_{AVG}Max was 0.08.

Dynamics of Rab5a on whole organelle during vesicle fusions

During infections with *wt Lm* and *hly- Lm*, we observed fusion events between *Lm*-containing vacuoles and macropinosomes or other *Lm*-containing vacuoles. Just after vacuoles contacted each other, total Rab5a and active Rab5a signals increased, mainly at the site of contact. After the vacuoles fused together, the Rab5 intensity increased over the newly formed vacuole, progressing in a wave-like motion from the point of contact. After levels of Rab5 had increased over the entire organelle, they again decreased.

Discussion

Here we used a combination of FRET and ratiometric microscopy to study Rab5, Cdc42, Rac1 and Rac2 activation patterns during macropinocytosis, phagocytosis of opsonized RBC and of *Lm* in murine macrophages, tostudy differences in the dynamics during endogenous homeostatic pathways and the effects *Lm* has on these during its uptake and survival. During RBC phagocytosis, Cdc42 localized to the front edge of the ruffle and was completely deactivated after closure. Rac1, Rac2 and Rab5 localized to the phagosome. The patterns of activation for Cdc42, Rac1 and Rac2 were similar to those reported in a previous study of RBC phagocytosis in RAW 264.7 cells (17). Rac1 localized to the forming phagosome prior to Rac2 and both were present on the phagosome until just after closure. Ratiometric imaging of CFP-Rab5 and mCherry showed that Rab5 also localized to the phagosome. Rab5 localization followed similar dynamics in BMM as in RAW 264.7, as previously shown (6). The activation values of Rab5 on the phagosome were lower than those on macropinosomes that formed in the same region of the cell.

Previous work by Yoshida, et al., (4), showed that, during M-CSF-stimulated macropinocytosis, Rac1 was activated but not Rac2. Here we observed that *Lm* activates a variety of signals during uptake. In contrast with RBC phagocytosis, where Cdc42 plays a role mostly on the edge of the ruffle, and macropinocytosis, where Cdc42 plays a similar role and Rac2 does not seem to be involved, all four GTPases were activated during *Lm* uptake. Cdc42 and Rac2 were activated during every *Lm* entry event. Interestingly, Rac1 localization and activation were observed on only a subset of BMM. It was previously shown that in murine BMM, *Lm* facilitates its uptake by activation of PI3K and Rac1 through toll-like receptor TLR2-MyD88 signaling (19). The diversity in Rab5 FRET levels on *Lm*-containing vacuoles within the same cell shows that *Lm* is able to modulate Rab5. Unfortunately, due to technical limitations we were unable to correlate FRET levels on individual *Lm*-containing vacuoles with *Lm* fate inside the macrophage. We hypothesize that *Lm* contained in vacuoles that showed low levels of Rab5 FRET would have a higher survival rate than *Lm* in vacuoles with higher Rab5 FRET levels. Vacuoles containing heat-killed *Lm* and *hly- Lm*, which does not express LLO, also showed low levels of Rab5 FRET. Functional LLO is missing in both of these conditions. Thus, damage of the BMM membrane by LLO could be a signal for activation of the phagocyte causing activation of Rab5 and localization of it to the vacuoles. Further studies will be carried out to understand the lack of Rab5 localization and activation in these cases.

The dynamics of Rab5 during fusion events show the complexity of Rab5 coordination. It points to two different levels of organization on the organelle; Rab5 levels are modified not only in the portion of the membrane where the fusion is occurring but also over the whole organelle.

These results show that *Lm* via some known and some still unknown virulence factors activates multiple pathways to enhance its probability of being taken up by macrophages. It activates all three studied small GTPases that are involved in the uptake stages of either macropinocytosis or phagocytosis and seems to be able to modulate Rac1 activity. After uptake we observe that unlike

during macropinocytosis and phagocytosis, where Rab5a activation values were constantly close to 10%, during Lm uptake there was considerable variation in the levels of activation reached by Rab5a, all within the first 3-5 minutes after uptake.

Figure 3.1. Cdc42, Rac1 and Rac2 Activation Patterns during RBC Phagocytosis. RBC phagosomes in BMM cells (A), showed activation of Cdc42 at the leading edge of the extending ruffle. Top row, phase-contrast; bottom row, EO [phase-contrast with overlay showing inactive YFP-Cdc42 (red) and active YFP-Cdc42 (green)], with the threshold for YFP-Cdc42 activation set at E_{AVG} = 8%. Rac1 localized to the RBC phagosome (B). Top row, phase-contrast; bottom row, EO [phase-contrast with overlay showing inactive YFP-Rac1 (red) and active YFP-Rac1 (green)], with the threshold for YFP-Rac1 activation set at E_{AVG} = 10%. Rac2 also localized to the forming phagosome (D). Top row, phase-contrast; bottom row, EO [phase-contrast with overlay showing inactive YFP-Rac2 (red) and active YFP-Rac2 (green)], with the threshold for YFP-Rac42 activation set at E_{AVG} = 12%. Scale bars = 5 μm.

Figure 3.1

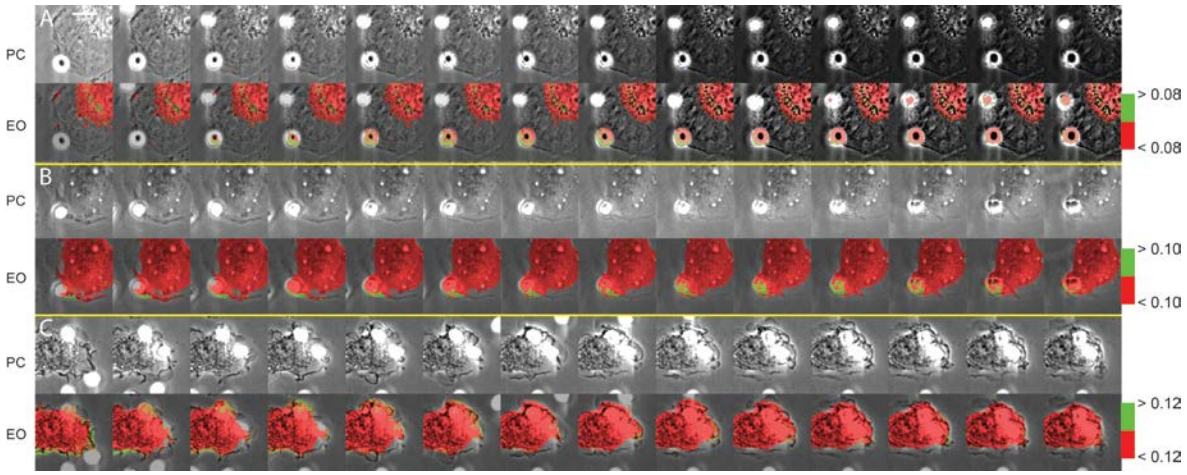

Figure 3.2. Cdc42, Rac1 and Rac2 Activation Patterns during Lm uptake.
Lm-containing vacuoles in BMM cells (A) showed activation of Cdc42 at the site of vacuole formation. Top row, phase-contrast; bottom row, EO [phase-contrast with overlay showing inactive YFP-Cdc42 (red) and active YFP-Cdc42 (green)], with the threshold for YFP-Cdc42 activation set at E_{AVG} = 8%. Rac1 localized to the *Lm*-containing vacuole in some cells (B), but was absent in others (C). Top row, phase-contrast; bottom row, EO [phase-contrast with overlay showing inactive YFP-Rac1 (red) and active YFP-Rac1 (green)], with the threshold for YFP-Rac1 activation set at E_{AVG} = 10% (B) and 8% (C). Rac2 localized to the forming vacuole (D). Top row, phase-contrast; bottom row, EO [phase-contrast with overlay showing inactive YFP-Rac2 (red) and active YFP-Rac2 (green)], with the threshold for YFP-Rac42 activation set at E_{AVG} = 12%. Scale bars = 3 μm.

Figure 3.2

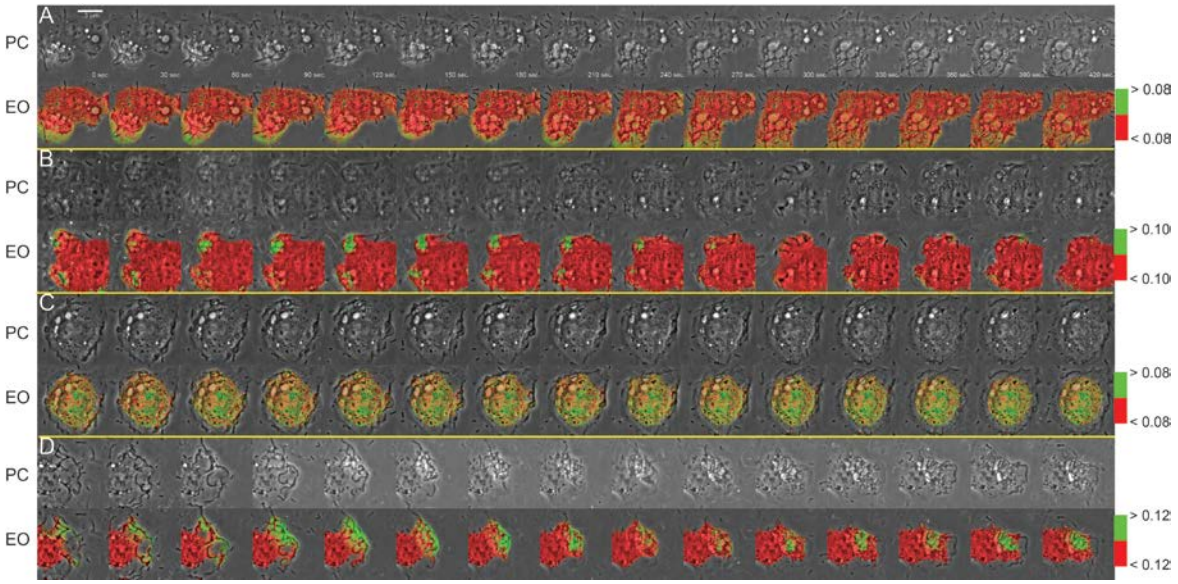

Figure 3.3. Differences in Rab5a activation levels during macropinocytosis and phagocytosis of RBC and *L. monocytogenes*. Rab5a localized to RBC phagosomes in BMM cells (A). Top row, phase-contrast; bottom row, EO [phase-contrast with overlay showing inactive CFP-Rab5a (red) and active CFP-Rab5a (green)], with the threshold for CFP-Rab5a activation set at E_{AVG} = 8%. Scale bars = 5 μm. During wt *Lm* uptake Rab5a localized to *Lm*-containing vacuole (B). Top row, phase-contrast; bottom row, EO [phase-contrast with overlay showing inactive CFP-Rab5a (red) and active CFP-Rab5a (green)], with the threshold for CFP-Rab5a activation set at E_{AVG} = 14%. Rab5a localized to *hly*- (C) and heat-killed *Lm*-containing (D) vacuoles with low levels of activation. Top row, phase-contrast; bottom row, EO [phase-contrast with overlay showing inactive CFP-Rab5a (red) and active CFP-Rab5a (green)], with the threshold for activation set at E_{AVG} = 5%. Scale bars = 3 μm.

Figure 3.3

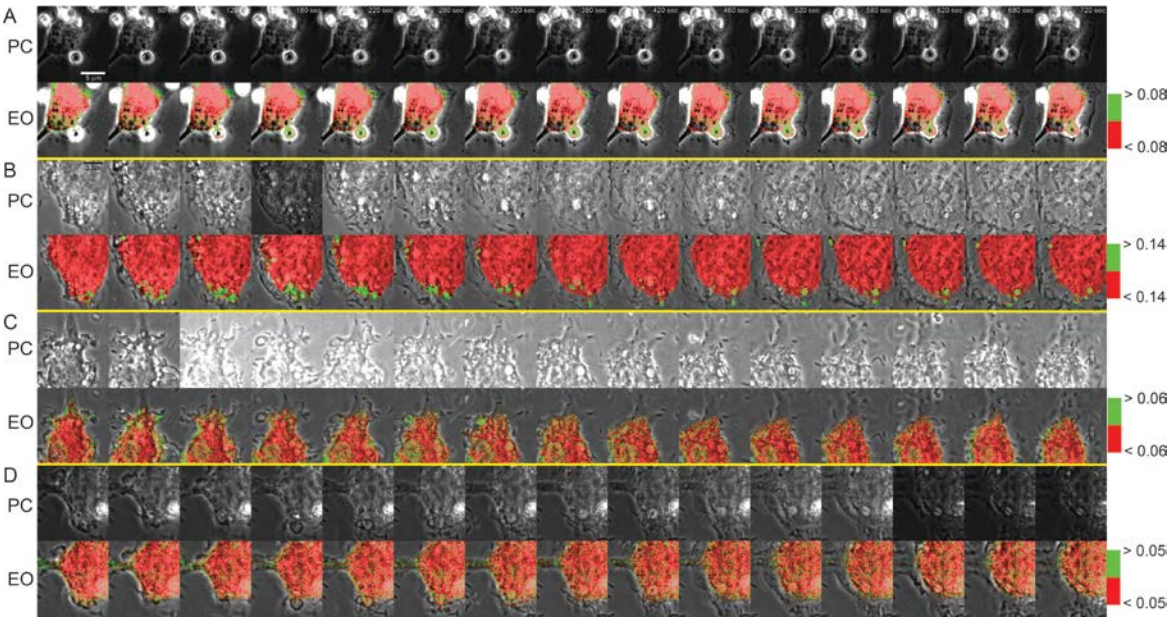

Figure 3.4. Dynamics of Rab5a on whole organelle during vesicle fusion. BMM transfected with YFP-Rab5a and CFP were infected with *wt Lm.* Two *Lm*-containing vacuoles come into contact and fuse causing an increase of Rab5a over the whole organelle (A). Top row, phase-contract; second row, YFP-Rab5a; third row, CFP fluorescence; bottom row, ratio of YFP-Rab5a to CFP. During uptake of *hly- Lm* a *Lm*-containing vacuole and an empty endosome come into contact and fuse, showing an increase in Rab5a ratio and a more localized increase in active Rab5a (B). Top row, phase-contrast; middle row, EO [phase-contrast with overlay showing inactive CFP-Rab5a (red) and active CFP-Rab5a (green)], with the threshold for CFP-Rab5a activation using a pseudocolor scale assigning different colors at 5% E_{AVG} steps (0 to 40% EAVG). Bottom row, ratio of CFP-Rab5a to mCherry (R_{CR}).

Figure 3.4

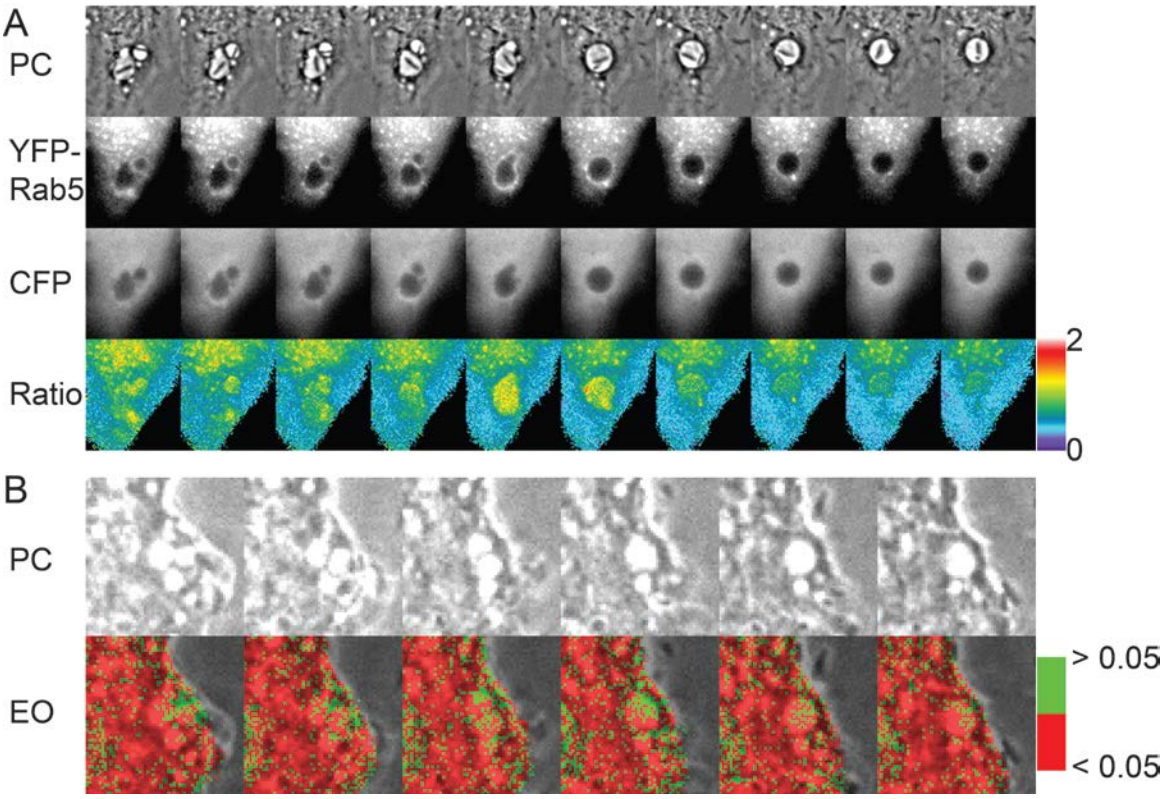

Bibliography

1. Prada-Delgado A, Carrasco-Marin E, Pena-Macarro C, Del Cerro-Vadillo E, Fresno-Escudero M, Leyva-Cobian F, Alvarez-Dominguez C. Inhibition of Rab5a exchange activity is a key step for Listeria monocytogenes survival. Traffic 2005;6(3):252-265.

2. Henry R, Shaughnessy L, Loessner MJ, Alberti-Segui C, Higgins DE, Swanson JA. Cytolysin-dependent delay of vacuole maturation in macrophages infected with Listeria monocytogenes. Cell Microbiol 2006;8(1):107-119.

3. Alvarez-Dominguez C, Barbieri AM, Beron W, Wandinger-Ness A, Stahl PD. Phagocytosed live Listeria monocytogenes influences Rab5-regulated in vitro phagosome-endosome fusion. J Biol Chem 1996;271(23):13834-13843.

4. Yoshida S, Hoppe AD, Araki N, Swanson JA. Sequential signaling in plasma-membrane domains during macropinosome formation in macrophages. J Cell Sci 2009;122(Pt 18):3250-3261.

5. Hoppe A, Christensen K, Swanson JA. Fluorescence resonance energy transfer-based stoichiometry in living cells. Biophys J 2002;83(6):3652-3664.

6. Henry RM, Hoppe AD, Joshi N, Swanson JA. The uniformity of phagosome maturation in macrophages. J Cell Biol 2004;164(2):185-194.

7. Parashuraman S, Mukhopadhyay A. Assay and functional properties of SopE in the recruitment of Rab5 on Salmonella-containing phagosomes. Methods Enzymol 2005;403:295-309.

8. Mukherjee K, Parashuraman S, Raje M, Mukhopadhyay A. SopE acts as an Rab5-specific nucleotide exchange factor and recruits non-prenylated Rab5 on Salmonella-containing phagosomes to promote fusion with early endosomes. J Biol Chem 2001;276(26):23607-23615.

9. Clemens DL, Lee BY, Horwitz MA. Deviant expression of Rab5 on phagosomes containing the intracellular pathogens Mycobacterium tuberculosis and Legionella pneumophila is associated with altered phagosomal fate. Infect Immun 2000;68(5):2671-2684.

10. Seabra MC, Mules EH, Hume AN. Rab GTPases, intracellular traffic and disease. Trends Mol Med 2002;8(1):23-30.

11. Hutagalung AH, Novick PJ. Role of Rab GTPases in membrane traffic and cell physiology. Physiol Rev 2011;91(1):119-149.

12. Scheper W, Zwart R, Sluijs P, Annaert W, Gool WA, Baas F. Alzheimer's presenilin 1 is a putative membrane receptor for rab GDP dissociation inhibitor. Hum Mol Genet 2000;9(2):303-310.

13. Cataldo AM, Peterhoff CM, Troncoso JC, Gomez-Isla T, Hyman BT, Nixon RA. Endocytic pathway abnormalities precede amyloid beta deposition in sporadic Alzheimer's disease and Down syndrome: differential effects of APOE genotype and presenilin mutations. Am J Pathol 2000;157(1):277-286.

14. Ravikumar B, Imarisio S, Sarkar S, O'Kane CJ, Rubinsztein DC. Rab5 modulates aggregation and toxicity of mutant huntingtin through macroautophagy in cell and fly models of Huntington disease. J Cell Sci 2008;121(Pt 10):1649-1660.

15. Alvarez-Dominguez C, Stahl PD. Increased expression of Rab5a correlates directly with accelerated maturation of Listeria monocytogenes phagosomes. J Biol Chem 1999;274(17):11459-11462.

16. Alvarez-Dominguez C, Madrazo-Toca F, Fernandez-Prieto L, Vandekerckhove J, Pareja E, Tobes R, Gomez-Lopez MT, Del Cerro-Vadillo E, Fresno M, Leyva-Cobian F, Carrasco-Marin E. Characterization of a Listeria monocytogenes protein interfering with Rab5a. Traffic 2008;9(3):325-337.

17. Hoppe AD, Swanson JA. Cdc42, Rac1, and Rac2 display distinct patterns of activation during phagocytosis. Mol Biol Cell 2004;15(8):3509-3519.

18. Swanson JA. Phorbol esters stimulate macropinocytosis and solute flow through macrophages. J Cell Sci 1989;94 (Pt 1):135-142.

19. Shen Y, Kawamura I, Nomura T, Tsuchiya K, Hara H, Dewamitta SR, Sakai S, Qu H, Daim S, Yamamoto T, Mitsuyama M. Toll-like receptor 2- and MyD88-dependent phosphatidylinositol 3-kinase and Rac1 activation facilitates the phagocytosis of Listeria monocytogenes by murine macrophages. Infect Immun 2010;78(6):2857-2867.

Chapter IV

Thesis Summary and Future Directions

Discussion

Summary of tools developed for this thesis

To understand the role of Rab5 during macropinocytosis and phagocytosis, I developed a set of tools that allowed both the study of Rab5 activation cycling *in vivo* and the modulation of its activity. The addition of a third fluorophore allowed simultaneous FRET and ratiometric microscopy studies in a single cell. Observing the interactions between YFP-RBD and CFP-Rab5, we were able to detect at which point during uptake Rab5 was in its active form. Co-expression of free mCherry via a pIRES2 vector served to localize total Rab5 by dividing CFP-Rab5 by mCherry. This ratiometric imaging does not differentiate between active and inactive forms of Rab5. Previously these two calculations would be obtained from two different cells, one expressing YFP-RBD and CFP-Rab5 and a second one expressing YFP-Rab5 and CFP. Combining both methods allowed me to observe the full cycle of Rab5 in distinct uptake pathways.

The pIRES2-mCherry vector contains an internal ribosome entry site between the multiple cloning site and the fluorescent protein, in this case mCherry, that allowed translation of a gene of interest and mCherry from a single bicistronic mRNA. We constructed a library of vectors expressing Rab5 GEFs and GAPs and constitutively active or dominant negative mutants of small GTPases Rac1, Rac2 and Cdc42, which are known to be involved in

macropinocytosis and phagocytosis. These allowed us to study the effect of interfering with the Rab5 cycle directly or indirectly.

Rab5 cycle dynamics and macropinosome size

Comparing the dynamics of D (total Rab5) and EDA (total FRET) showed that during the early events of Rab5 association and activation, both signals increase simultaneously for all macropinosomes regardless of size. The second part of the cycle, which includes the deactivation and dissociation of Rab5 from the membrane, showed the EDA signal decreasing faster than the D signal, again regardless of size. These findings indicate a difference with the current model of Rab5 cycle on the membrane, which proposes a delay between the association and the activation steps during formation of the macropinosome (1). Another finding of this study is the relation between total Rab5 cycle time and the diameter of the forming macropinosome. On most macropinosomes with diameters larger than 4 μm, Rab5 required longer to cycle fully. This size relationship was observed mainly during the deactivation and dissociation part of the cycle. This relation shows a possible mechanism used by the cell to detect size of the macropinosome, where larger macropinosomes are delayed in their maturation while it is reduced in size by mechanisms such piranhalysis or kiss-and-run until it reaches a proper size to continue along the maturation pathway.

Effect of Rab5 GEF expression and acidification inhibition on macropinosome formation

Macropinosomes from cells expressing a pIRES2-mCherry construct with GEFs Rin1 or Rabex-5 retained active Rab5 (EDA) for a longer period of time. These macropinosomes also reached a higher peak level of Rab5 FRET when compared with control macropinosomes. Another finding was that these cells had an increased number of Rab5 FRET-positive tubules. A similar phenotype was observed when treating cells with bafilomycin A1, which inhibits acidification

of endosomes, these cells contained a large number of Rab5 FRET-positive tubules stretching outwards from the nucleus. This shows a relation between Rab5 ability to cycle and macropinosome acidification and maturation. This may be related to the extension of endosomal membrane by microtubules, where Rabenosyn-5, a Rab5 effector is known to play a role (2). Also, this effect could be due to the inability of the macropinosome to fuse with the lysosome, some pathogens known to target Rab5 and modulate its activation cycle have been shown to form similar elongated tubules at different points during its uptake and maturation of the pathogen-containing vesicle (eg., *Salmonella*) (add REFs). The different studies looked at particular Rabs and different time intervals and have observed that different Rabs localize to those tubules.

Rab5 activation required for formation of a stable macropinosome.

Cells expressing dominant negative Rab5 or cells expressing pIRES2-mCherry-RabGAP-5 showed similar phenotypes, in which macropinosomes began to form but were unable to form a fully round macropinosome. After a couple of minutes these unstable macropinosomes disappeared, presumably by fusing back with the membrane. Although dominant negative Rab5 does not localize to membrane, we did observe in cells expressing YFP-RBD, CFP-Rab5 and pIRES2-mCherry-RabGAP-5 a low level of recruitment of Rab5; however, Rab5 activation levels were negligible. These findings, in conjunction with the ones obtained from expression of GEFs and treatment with bafilomycin A1, indicate roles for Rab5 in tubule formation and macropinosome stability.

Activation patterns of Cdc42, Rac1, Rac2 and Rab5 during phagocytosis in macrophages

Murine primary bone marrow-derived macrophages transfected with YFP chimeras of Cdc42, Rac1 or Rac2 and CFP-PBD were fed E-IgG-opsonized sheep red blood cells and the localization and activation patterns were calculated

and compared to previously published results on macrophage-like cell line RAW 264.7. One difference between cells is that bone marrow-derived macrophages, unlike RAW cells, spread thinly on coverslips. Consequently, in all the phagocytosis events the RBC landed on top of the cell and the cell engulfed them from the bottom up. The RBC covered part of the early cup forming signals. In RAW cells, many of the phagocytosis events were side-views, which showed similar patterns of localization and activation, where Cdc42 localized to the tip of the membrane ruffle and did not localize to the phagosome (REF). Rac1 localized to the phagosome just before the phase-dark transition but lasted until after closure. Rac2 also localized to the cup and followed the leading edge of the ruffle and peaking at closure. On macrophages expressing YFP-RBD and CFP-Rab5, Rab5 peaked at or just after closure. The levels of Cdc42, Rac2 and Rab5 FRET during RBC phagocytosis were in the range of 15% (ie., E_{AVG} = 0.15), whereas the levels of Rac1 FRET reached close to 25% at its maximum point.

Activation patterns of small GTPases during Lm uptake

I worked out a protocol to observe *Lm* uptake by macrophages. Cdc42 and Rac2 localized to the ruffle where *Lm* was taken up. In the literature there are two opposing findings involving Rab5 localization to the *Lm*-containing vacuole. Henry, et. al. (3) did not observe localization of Rab5 to the *Lm*-containing vacuoles. Alvarez-Dominguez, et al., (4), using macrophage-like J774E cells, did observe localization. In primary macrophages transfected with YFP-Rab5 and CFP, Rab5 localized to the *Lm*-containing vacuole. Using the YFP-RBD/CFP-Rab5 FRET system, we studied how *Lm* modulates Rab5 activation to survive in the host. As stated above, many pathogens target Rab5 activation, either by keeping Rab5 inactive to delay vesicle maturation, or by keeping Rab5 in its active form, eliciting continuous fusion with endosomes and delaying fusion with lysosomes. Prada-Delgado, et al., (5) found that *Lm* modulates Rab5 activity by keeping it in its inactive form. Our FRET data showed a mixed population of *Lm*-containing vacuoles, some vacuoles had very

low to no FRET signal while others showed a strong FRET signal. This mixed population is expected since not every bacterium survives. Currently I have been trying to develop a method to follow single bacteria through the pathway, to see if the vacuoles with low to no FRET are the ones that allow *Lm* to survive and continue infection.

Rac1 activation patterns during *Lm* uptake were surprising. Rac1 localized to vacuoles in some cells and not in others. This suggests that *Lm* is somehow also able to modulate Rac1 activation. Also, this shows that unlike RBC phagocytosis, where Cdc42 is restricted to the leading edge of the ruffle, or M-CSF-stimulated macropinocytosis, where neither Cdc42 nor Rac2 are involved, all four small GTPases are involved in *Lm* uptake.

Rab5 activity during uptake of hly- and heat-killed Lm

In contrast to wild type *Lm* uptake, where we observed variable levels of Rab5 FRET on the *Lm*-containing vacuoles, all of the vacuoles containing *hly*- or heat-killed *Lm* showed low FRET levels. This finding suggests a possible role of LLO damage to the membrane as a mechanism for modulation of the Rab5 cycle by *Lm*.

Rab5 dynamics during fusion

We also observed fusion events during *Lm* infection of BMM transfected with YFP-Rab5a and CFP. As described previously (6), the highest Rab5 concentration localized to the point of contact between both vesicles. Interestingly we observed that, during vacuole fusion with macropinosomes, YFP-Rab5 did not just localize to the point of contact. Instead, Rab5 levels on the whole organelle increased, beginning at the point of contact and radiating over the new vacuole. Similar events were observed during uptake of *hly- Lm* in BMM transfected with YFP-RBD, CFP-Rab5 and mCherry. The ratio of CFP-Rab5 to mCherry showed localization of Rab5 and an overall increase in vacuole labeling

with Rab5. The FRET data showed a similar increase in FRET with the highest levels of FRET localizing to the point of contact. These are interesting observations that support a larger regulatory control in the cell. Rab5 activity is not just localized to points of contact between vesicles, but rather has a cascading result over the whole organelle.

I want to note that three different FRET probes were made. The first probe consisted of the carboxy-terminus of EEA1. Because we later found that it also contained a FYVE domain and bound PI3P with higher affinity than Rab5, we did not study it further. The second probe was the Rab5-binding domain of Rab5 effector, Rabaptin-5, a gift from Dr. Alexander Sorkin's Lab (University of Pittsburgh). It showed similar patterns of FRET to the third probe we made, the amino-terminus RBD of EEA1, but showed a lower affinity to active Rab5.

Future Directions

My thesis work involved the creation of different tools and methods to study the activation patterns of small GTPases, concentrating on Rab5 activities during uptake events. Two new FRET probes for Rab5 were developed. FRET and ratiometric microscopy were analyzed in single cells. A pIRES2 expression library of the principal GTPases and Rab5 GAPs and GEFs allowed for modulation of the cycle parameters and coincident monitoring of the Rab5 cycle parameters. These methods allowed analysis of Rab5 dynamics during uptake of *Lm* and the early stages of the infection in macrophages. These tools should facilitate study of how different pathogens affect Rab5 *in vivo*, how they affect its activity and at what point they interfere with Rab5 function. As Rab5 is involved in the initial part of most endocytic events, a better understanding its dynamics should lead to better tools to combat the increasing number of pathogens that target Rab5. It may also lead to better drugs to treat the increasing number of diseases known to have Rab5 defects as one of their major causes.

Follow-up experiments

With these new tools we obtained results that lead us to many follow-up questions.

Macropinocytosis

In figure 2.2 we observed that on macropinosomes larger than 4 μm in diameter Rab5 took longer to cycle fully. I hypothesize that cells are able to sense the size of a macropinosome and delay Rab5 cycling when the vacuole is too large to enter directly into the endocytic pathway. By slowing the Rab5 cycle it might allow vesicle budding and events such as kiss and run, reducing the cargo and thus the size of the vacuole until it is able to continue down the pathway. As a consequence of the cycle delay we expect that the acidification of the macropinosome will also be delayed, using a pH-sensitive fluorescent dye we can pulse and chase measuring the pH values through time of different size macropinosomes.

Treatment of cells with bafilomycin A1, which inhibits acidification of macropinosomes by inhibiting vacuolar proton ATPases, destabilized the Rab5 cycle and increased the number of Rab5 FRET-positive tubules. The cell membrane does not contain vacuolar proton ATPases and it is not yet fully understood how macropinosomes acquire these. One possibility is that the Rab5 FRET-positive tubules which are also observed to a lesser degree in untreated cells are the source of V-ATPases and that the lack of them causes the Rab5 cycle to destabilize. Using commercially available antibodies against V-ATPases such as E11 (directed against the E subunit of V-ATPase; (7-10)) we can observe their localization during the early events of macropinocytosis. My hypothesis is that recently formed macropinosomes lack V-ATPase and that the Rab5 FRET-positive tubules contain high concentrations of V-ATPase. It has also been observed that different pathogens such as *Salmonella* have been found in tubule-like structures positive for different Rabs (Salmonella-induced filaments, or SIFs; (11)). I hypothesize that since Rab5 functions during the early

stages of pathogen uptake and *Salmonella* modulates Rab5 by keeping it in its active form, that SIFs are Rab5-positive during part of the early formation. Also, we can compare acidification of this structure and V-ATPase concentration.

Our data showed that activation of Rab5 occurs almost simultaneously with Rab5 association with the membrane and that dissociation of Rab5 from the membrane happens at a slower rate than deactivation. We also observed that expression of YFP-RBD did not affect the Rab5 association rate, but did slow the dissociation rate. It is possible that this lag observed between deactivation and dissociation is due to the Rab5-binding domain interfering with Rab5 effectors such as GDI, consequently delaying the removal of Rab5 from the membrane. Rab5 forms complexes with different effectors and other Rabs (6, 12-16) . Although the RBD leaves and is not close enough to give a FRET signal during deactivation, it could nonetheless impede access of GDI to the complex. To study this possibility, we could express a red fluorescent chimera of GDI to study its dynamics during macropinocytosis and its effect on dissociation of Rab5. My hypothesis is that if the RBD is affecting the dissociation event, either by being stuck within the complex or by its overexpression being too high compared to endogenous GDI levels, the lag observed would decrease or fully disappear.

Expression of dominant negative Rab5 or overexpression of RabGAP-5 caused an increase in unstable macropinosomes. Requirement of Rab5 cycling for stabilization of the macropinosome could indicate a regulatory circuit between Rab5 and actin. Recently it was published that active Rab5 interacts with L- and T-plastin which are actin-binding proteins involved in regulation of cell morphology, tumor progression, bacterial invasion and lamellopodium protrusion (17-19). There are no studies looking at plastin's role during macropinocytosis, but it is known that macrophages express them. I hypothesize that plastins are involved in macropinosome formation and that by keeping Rab5 inactive the interaction between Rab5 and plastin is blocked causing the destabilization of the macropinosome. Fluorescent chimeras of plastin proteins have been used and published already (18).

Listeria monocytogenes

Another interesting result was the differences in Rab5 activation levels observed in cells expressing wild-type *Listeria* (0-15%) and *hly*- and heat-killed *Listeria* (8%). The main difference between these conditions was the lack of listeriolysin O activity in *hly*- and heat-killed *Lm*. This suggests a role for LLO during Rab5 modulation, possibly by forming pores on the vacuole membrane that allow a virulence factor to access the cytoplasm. These observations are opposite to the findings by Alvarez-Dominguez, et. al., (20) where LLO was found not to be critical for virulence factor p40 effect on Rab5.

It is possible that LLO released by *Lm* to the media is causing damage on the cell membrane and allowing the passage of virulence factors that otherwise would be produced inside the vacuole after *Lm* uptake and this is causing the differences in FRET levels or the timing of these effects on Rab5. Macrophages incubated with wild-type *Lm* ruffled more and took up more bacteria than those incubated with heat-killed or *hly*- strains. LLO might have a role on inducing or enhancing ruffling and macropinocytosis on macrophages to increase the chances of *Lm* uptake. This possibility can be tested by addition of purified LLO to the media at different concentrations.

One technical limitation we encountered was not being able to follow single *Lm*–containing vacuoles with different levels of FRET through time to identify if those with lower levels of FRET had an increased survival rate. One way we could test this is by creating a *Lm* that expresses a photoactivatable red fluorophore. Using the 4D microscope at the Center for Live Cell Imaging, we could incubate macrophages expressing YFP-RBD and CFP-Rab5 with wild-type photoactivatable *Lm*, observe uptake, photoactivate proteins inside the *Lm* contained in that vacuole, then observe whether it escapes or remains contained in the vacuole.

Another option is the use of a commercially available pH-dependent red fluorescent mKate variant (21). Inserting this fluorophore in a bacterial plasmid and creating an mKate-expressing *Lm* would allow us to determine not only the

fate of *Lm*-containing vacuoles with different Rab5 FRET levels, but also to observe the changes in vacuole pH. This would allow us to determine f there is an optimal pH at which escape occurs, similar to the earlier studies of Beauregard et al. (22)and Shaughnessy et al. (23).

Pathogenesis and *Neurological diseases*

As the list of pathogen virulence factors, and neurological diseases and cancers implicating Rab5 increases, the use of these tools should prove to be useful for their study *in vivo* to better understand the sequence of events and dynamics that these modulations or mutations cause. Being able to look at these events should lead to a more complete map of where and when major pathways are affected. This could facilitate the selection of possible therapeutic targets for treatments. Finally the fact that different pathogens target specific Rab5 isoforms makes these FRET probes more valuable since the RBD binds all three isoforms with high affinity.

Bibliography

1. Rybin V, Ullrich O, Rubino M, Alexandrov K, Simon I, Seabra MC, Goody R, Zerial M. GTPase activity of Rab5 acts as a timer for endocytic membrane fusion. Nature 1996;383(6597):266-269.

2. Nielsen E, Christoforidis S, Uttenweiler-Joseph S, Miaczynska M, Dewitte F, Wilm M, Hoflack B, Zerial M. Rabenosyn-5, a novel Rab5 effector, is complexed with hVPS45 and recruited to endosomes through a FYVE finger domain. J Cell Biol 2000;151(3):601-612.

3. Henry R, Shaughnessy L, Loessner MJ, Alberti-Segui C, Higgins DE, Swanson JA. Cytolysin-dependent delay of vacuole maturation in macrophages infected with Listeria monocytogenes. Cell Microbiol 2006;8(1):107-119.

4. Alvarez-Dominguez C, Barbieri AM, Beron W, Wandinger-Ness A, Stahl PD. Phagocytosed live Listeria monocytogenes influences Rab5-regulated in vitro phagosome-endosome fusion. J Biol Chem 1996;271(23):13834-13843.

5. Prada-Delgado A, Carrasco-Marin E, Pena-Macarro C, Del Cerro-Vadillo E, Fresno-Escudero M, Leyva-Cobian F, Alvarez-Dominguez C. Inhibition of Rab5a exchange activity is a key step for Listeria monocytogenes survival. Traffic 2005;6(3):252-265.

6. Eitzen G, Will E, Gallwitz D, Haas A, Wickner W. Sequential action of two GTPases to promote vacuole docking and fusion. Embo J 2000;19(24):6713-6720.

7. Yoshimori T, Yamamoto A, Moriyama Y, Futai M, Tashiro Y. Bafilomycin A1, a specific inhibitor of vacuolar-type H(+)-ATPase, inhibits acidification and protein degradation in lysosomes of cultured cells. J Biol Chem 1991;266(26):17707-17712.

8. D'Arrigo A, Bucci C, Toh BH, Stenmark H. Microtubules are involved in bafilomycin A1-induced tubulation and Rab5-dependent vacuolation of early endosomes. Eur J Cell Biol 1997;72(2):95-103.

9. Bayer N, Schober D, Prchla E, Murphy RF, Blaas D, Fuchs R. Effect of bafilomycin A1 and nocodazole on endocytic transport in HeLa cells: implications for viral uncoating and infection. J Virol 1998;72(12):9645-9655.

10. Mesaki K, Tanabe K, Obayashi M, Oe N, Takei K. Fission of tubular endosomes triggers endosomal acidification and movement. PLoS One 2011;6(5):e19764.

11. Brumell JH, Tang P, Mills SD, Finlay BB. Characterization of Salmonella-induced filaments (Sifs) reveals a delayed interaction between Salmonella-containing vacuoles and late endocytic compartments. Traffic 2001;2(9):643-653.

12. Ullrich O, Stenmark H, Alexandrov K, Huber LA, Kaibuchi K, Sasaki T, Takai Y, Zerial M. Rab GDP dissociation inhibitor as a general regulator for the membrane association of rab proteins. J Biol Chem 1993;268(24):18143-18150.

13. Ullrich O, Horiuchi H, Bucci C, Zerial M. Membrane association of Rab5 mediated by GDP-dissociation inhibitor and accompanied by GDP/GTP exchange. Nature 1994;368(6467):157-160.

14. Mukherjee K, Siddiqi SA, Hashim S, Raje M, Basu SK, Mukhopadhyay A. Live Salmonella recruits N-ethylmaleimide-sensitive fusion protein on phagosomal membrane and promotes fusion with early endosome. J Cell Biol 2000;148(4):741-753.

15. Seabra MC, Wasmeier C. Controlling the location and activation of Rab GTPases. Curr Opin Cell Biol 2004;16(4):451-457.

16. Liu P, Bartz R, Zehmer JK, Ying YS, Zhu M, Serrero G, Anderson RG. Rab-regulated interaction of early endosomes with lipid droplets. Biochim Biophys Acta 2007;1773(6):784-793.

17. Zhou DH, Yuan ZG, Zhao FR, Li HL, Zhou Y, Lin RQ, Zou FC, Song HQ, Xu MJ, Zhu XQ. Modulation of mouse macrophage proteome induced by Toxoplasma gondii tachyzoites in vivo. Parasitol Res 2011.

18. Al Tanoury Z, Schaffner-Reckinger E, Halavatyi A, Hoffmann C, Moes M, Hadzic E, Catillon M, Yatskou M, Friederich E. Quantitative kinetic study of the actin-bundling protein L-plastin and of its impact on actin turn-over. PLoS One 2010;5(2):e9210.

19. Hagiwara M, Shinomiya H, Kashihara M, Kobayashi K, Tadokoro T, Yamamoto Y. Interaction of activated Rab5 with actin-bundling proteins, L- and T-plastin and its relevance to endocytic functions in mammalian cells. Biochem Biophys Res Commun 2011;407(3):615-619.

20. Alvarez-Dominguez C, Madrazo-Toca F, Fernandez-Prieto L, Vandekerckhove J, Pareja E, Tobes R, Gomez-Lopez MT, Del Cerro-Vadillo E, Fresno M, Leyva-Cobian F, Carrasco-Marin E. Characterization of a Listeria monocytogenes protein interfering with Rab5a. Traffic 2008;9(3):325-337.

21. Wang Q, Byrnes LJ, Shui B, Rohrig UF, Singh A, Chudakov DM, Lukyanov S, Zipfel WR, Kotlikoff MI, Sondermann H. Molecular Mechanism of a Green-Shifted, pH-Dependent Red Fluorescent Protein mKate Variant. PLoS One 2011;6(8):e23513.

22. Beauregard KE, Lee KD, Collier RJ, Swanson JA. pH-dependent perforation of macrophage phagosomes by listeriolysin O from Listeria monocytogenes. J Exp Med 1997;186(7):1159-1163.

23. Shaughnessy LM, Hoppe AD, Christensen KA, Swanson JA. Membrane perforations inhibit lysosome fusion by altering pH and calcium in Listeria monocytogenes vacuoles. Cell Microbiol 2006;8(5):781-792.

Appendix

DNA Constructs prepared for these studies:

Clontech C1 and N1 vectors for all constructs, these contain a human cytomegalovirus (CMV) promoter and a kanamycin and neomycin resistance gene.

pIRES constructs were made using Clontech's pIRES2-EGFP vector, which contains a human cytomegalovirus (CMV) promoter, a kanamycin and neomycin resistance gene and an internal ribosome entry site (IRES) of the encephalomyocarditis virus. The multiple cloning site (MCS) is followed by the IRES site and finally the fluorescent protein.

Cerulean-Rab5a

mCherry-Rab5a

YFP-Rab5b

CFP-Rab5b

Cerulean-Rab5b

mCherry-Rab5b

YFP-Rab5c

CFP-Rab5c

Cerulean-Rab5c

mCherry-Rab5c

mCherry-Rab7

mCherry-Rab7(T22N)

mCherry-Lamp1

mCherry-EEA1

YFP-RBD (Amino-terminal of EEA1, aa 36-218)

CFP-RBD (Amino-terminal of EEA1)

Cerulean-RBD (Amino-terminal of EEA1)

mCherry-RBD (Amino-terminal of EEA1)

CFP- RBDFYVE (Carboxy-terminal of EEA1 (aa 1257-1411), contains a FYVE domain)

Cerulean- RBDFYVE (Carboxy-terminal of EEA1, contains a FYVE domain)

mCherry- RBDFYVE (Carboxy-terminal of EEA1, contains a FYVE domain)

R5BD-YFP (Rabaptin-5 Rab5-binding domain, aa 551-862)

R5BD-CFP (Rabaptin-5 Rab5-binding domain)

R5BD-Cerulean (Rabaptin-5 Rab5-binding domain)

R5BD-mCherry (Rabaptin-5 Rab5-binding domain)

YFP-R5BD (Rabaptin-5 Rab5-binding domain, no FRET in N1 vector)

CFP-R5BD (Rabaptin-5 Rab5-binding domain, no FRET in N1 vector)

Cerulean-R5BD (Rabaptin-5 Rab5-binding domain, no FRET in N1 vector)

mCherry-R5BD (Rabaptin-5 Rab5-binding domain, no FRET in N1 vector)

pIRES2-CFP-Rab5(S34N)

pIRES2-mCherry

pIRES2-mCherry-Rin1

pIRES2-mCherry-Rabex-5

pIRES2-mCherry-RabGAP-5

pIRES2-mCherry-Arf6

pIRES2-mCherry-Arf6(Q67L)

pIRES2-mCherry-Arf6(T27N)

pIRES2-mCherry-Cdc42

pIRES2-mCherry-Cdc42(V12)

pIRES2-mCherry-Cdc42(N17)

pIRES2-mCherry-Rac1

pIRES2-mCherry-Rac1(V12)

pIRES2-mCherry-Rac1(Q71)

pIRES2-mCherry-Rac1(N17)

pIRES2-mCherry-Rac2

pIRES2-mCherry-Rac2(V12)

pIRES2-mCherry-Rac2(N17)

mCherry-p85α

Dyn2-mCherry

Dyn2(K44A)-mCherry

Dyn2ΔPRD-mCherry